UNIVERSITY OF CALIFORNIA

Los Angeles

Spectral Modulation of Upconversion Emissions with Composition Tuning and Surface Plasmonic Resonance

A dissertation submitted in partial satisfaction of the requirements for the degree Doctor of Philosophy in Materials Science and Engineering

by

Hua Zhang

2013

ABSTRACT OF THE DISSERTATION

Spectral Modulation of Upconversion Emissions

with Composition Tuning

and Surface Plasmonic Resonance

by

Hua Zhang

Doctor of Philosophy in Materials Science and Engineering

University of California, Los Angeles, 2013

Professor Yu Huang, Chair

Rare-earth doped upconversion nanocrystals (UCNCs) have lately drawn much attention in different fields such as solar cells, biolabeling and display technologies due to their unique ability to convert lower energy photons into high energy photons and the associated advantages. For example, with an IR excitation, UCNCs can function as effective biolabels with very large sample penetration depth, high photostability and high signal-to-noise ratio. The ability to achieve this shorter wavelength emission through an upconversion process is of significance for activating certain chemical or biological processes. Therefore, it is important that the emission wavelength can be tuned and

enhanced by various approaches.

In this dissertation, the spectral modulation of upconversion emissions has been achieved by both changing the dopant concentration and coupling the upconversion nanocrystals with noble metal nanostructures (i.e. surface plasmonic resonance). The relative spectral intensity can be tuned from 0.5 to 3 and the single wavelength emission can be enhanced by over 12 fold.

These findings open a new pathway to rationally modulate the upconversion emission, and can broadly impact in areas including biomedical imaging, sensing and therapeutics, as well as enable new opportunities for energy harvesting and conversion.

The dissertation of Hua Zhang is approved.

Qibing Pei

Yang Yang

Xiangfeng Duan

Yu Huang, Committee Chair

University of California, Los Angeles

2013

Table of Contents

Vita

2008 B.S. Materials Science

Fudan University Shanghai, China

Chapter 1 Introduction

1.1 Introduction to upconversion nanocrystals

When a medium emits fluorescence as a result of being excited by incident light, the wavelength of the fluorescence is usually longer than that of the excitation light, which is called the energy down conversion process. However, under some special circumstances one can obtain emitted light with wavelength shorter than that of the excitation light through an energy upconversion process.[1-4] This process can be realized in three possible schemes (Fig. 1-1): (1) two-photon absorption excitation, which involves a non-stationary quantum mechanical state; (2) excited state absorption, in which a first absorption process leads to an intermediate excited level, from where further absorption leads to higher levels; (3) energy transfer between two active centers, where two centers in an intermediate level interact to generate one center at a higher level while the other one gets de-excited. Among the three schemes, the first one (two photon absorption) involves a virtual quantum mechanical state and has extremely low efficiency ($<10^{-10}$); While both the excited state absorption and energy transfer process involve metastable intermediate states, and can have much higher upconversion efficiency. In particular, the energy transfer upconversion process can be very efficient ($\sim10^{-1}$) if an energy resonance exists between two centers.[1] Rare earth element doped materials are among the most promising materials for energy upconversion because they have multiple long-lived (>μs) excited states.[5-7]

This unique property makes upvonersion materials attractive for a wide range of

applications. In particular, nanostructures made from energy upconversion materials are of considerable interest due to their potential for biomedical imaging and therapeutics.[8-11] The fact that they can be excited with infrared light makes them attrative candidates as biological probes for deeper imaging with lower noise, in contrast to traditional organic dyes and quantum dots.[12-15] Er-Yb or Tm-Yb co-doped $NaYF_4$ are among the most efficient energy upconversion materials, in which ~50% of absorbed IR photons can be converted to visible photons due to nearly perfect resonance between these color centers.[16] Depending on the exact energy levels involved, Yb, Er or Tm co-doped $NaYF_4$ upconversion material can convert IR photons (e.g. 980 nm) to a wide range of shorter wavelength color including violet, blue, green and red (Fig. 1-2).[16] The luminescence spectra of these materials are typically characterized by sharp peaks with specific spectral positions determined by the 4f electron energy levels, and are in general independent of host matrix (let it be a crystal, a glass, or even polymer).

Recently, considerable efforts have been devoted to the synthesis of energy upconversion nanoparticles.[17,18] The energy upconversion NCs can be synthesized using colloidal growth approach employing organic capping ligand.[19-21] For example, to synthesize Yb-Tm co-doped yttrium fluoride nanoparticles, we can dissolve YCl_3, $YbCl_3$ and $TmCl_3$ together in ligand/solvent such as oleic acid/oleic amine with a proper ratio and then inject into a re-circulating flask of $Na(CF_3COO)$ solution. By tuning the reaction temperature, precursor/capping-ligand ratio or concentration, one can rationally tailor the size, size distribution, morphology, crystal structure and dopant concentrations in Yb-Tm

co-doped yttrium fluoride nanoparticles $NaYF_4$:Re (Re=Yb, Tm). Indeed, our preliminary studies have shown that (Yb-Er) or (Yb-Tm) co-doped nanoparticles can emit multiple different colors (red, green, blue or violet) that can be readily varied by adjusting the exact doping ratio or preparation conditions (Fig. 1-3).

Rare earth elements (e.g. Er, Yb, Tm) doped materials can exhibit interesting energy upconversion properties to convert IR photons into visible photons. The ability to tune the spectral properties of such materials is of significant interest for photon energy conversion that may lead to interesting opportunities in organic photovoltaics (to convert IR photons into visible photons for organic photovoltaics) or photocatalytic reactions, as well as for biomedical imaging and therapeutics.

1.2 Introduction to surface plasmonic resonance

Surface plasmon resonance is the collective electron cloud oscillation on a metal surface or nanoparticle (NP) caused by its interaction with incident light.[22,23] This leads to a number of interesting optical events such as the absorption and scattering of photons of certain wavelength and is responsible for the wide range of colors observed in metal NP colloids.[24,25] Additionally, the large local electrical fields generated by SPR in the vicinity of the NPs can significantly modify the spectroscopic properties of neighbouring fluorophores.[26-31] SPR is largely responsible for surface enhanced Raman spectroscopy (SERS) with an enhancement factor of up to 10^{14}-10^{15}, allowing the technique to be sensitive enough for single molecule detection.[32-34]

Nanoscale integration of multiple functional components can enable exciting new opportunities to precisely control and fine tune the electronic and optical properties of the resulting materials. Recently, gold and silver NPs, or islands, have been explored to enhance the fluorescent emission of various nanostructures such as semiconductor quantum dots or fluorescent molecules.[35-38] In general, the origin of plasmonic enhancement may be fundamentally attributed to two major origins: (1) an increase of excitation rate by local field enhancement (LFE): an enhancement of effective excitation flux caused by local field enhancement associated with plasmonic resonance; (2) an increase of emission rate by surface plasmon coupled emission (SPCE): an enhancement of emission efficiency due to the coupling of the upconversion emission with the NP plasmonic resonance which will effectively increase both the non-radiative and radiative decay rate. SPCE can occur when the emission band of the fluorophore overlaps with the plasmon resonance frequency of the metal nanostructures,[39] and LFE may play important role when the plasmon resonance frequency overlaps with the excitation wavelength. In many systems, both factors contribute to the fluorescence enhancement and are extremely sensitive to the relative spectral position of excitation and emission spectra of the fluorophores and plasmonic resonance frequency of metallic nanostructures.[36,39] However, it is often difficult to differentiate the effects of excitation enhancement and emission rate enhancement, especially in traditional organic dyes with overlap in the excitation and emission spectra.

While in upconversion nanocrystals (NCs) that are able to convert lower energy

photons (typically near-infrared (NIR)) into higher energy photons (usually visible), the excitation and emission spectra can be substantially different and usually don't have significant overlap[1]. It therefore can allow investigation of the interplay between the excitation-plasmonic resonance or emission-plasmonic resonance separately, and distinguish their effect on the fluorescence enhancement. Additionally, based on the fact that different upconversion emission peaks were result from different numbers of photons involved, power dependence studies may also offer critical insight into the LFE effect.

References

1. Auzel, F., Upconversion and anti-stokes processes with f and d ions in solids. *Chemical Reviews* 104 (1), 139-173 (2004).
2. Gamelin, D.R. & Gudel, H.U., Upconversion processes in transition metal and rare earth metal systems in *Transition Metal and Rare Earth Compounds: Excited States, Transitions, Interactions Ii* (2001), Vol. 214, pp. 1-56.
3. Vetrone, F. & Capobianco, J.A., Lanthanide-doped fluoride nanoparticles: luminescence, upconversion, and biological applications. *Int. J. Nanotechnol.* 5 (9-12), 1306-1339 (2008).
4. Wang, F. & Liu, X.G., Recent advances in the chemistry of lanthanide-doped upconversion nanocrystals. *Chemical Society Reviews* 38 (4), 976-989 (2009).
5. Sandrock, T., Scheife, H.; Heumann, E., Huber, G. High-power continuous-wave upconversion fiber laser at room temperature. Opt. Lett. 1997, 22, 808-810.

6. Downing, E., Hesselink, L., Ralston, J., Macfarlane, R. A three-color, solid-state, three-dimensional display. Science. 1996, 273, 1185-1189.
7. Joubert, M.F. Photon avalanche upconversion in rare earth laser materials. Optical Materials. 1999, 11, 181-203.
8. S. F. Lim, R. Riehn and W. S. Ryu, N. Khanarian, C. K. Tung, D. Tank, R. H. Austin, Nano Lett., 2006, 6, 169.
9. D. K. Chatterjee, A. J. Rufaihah and Y. Zhang, Biomat., 2008, 29, 937.
10. D. K. Chatterjee, L. S. Fong and Y. Zhang, Advanced Drug Delivery Reviews., 2008, 60, 1627.
11. L. Y. Wang, R. X. Yan, Z. Y. Huo, L. Wang, J. H. Zeng, J. Bao, X. Wang, Q. Peng and Y. D. Li, Angew. Chem. Int. Ed., 2005, 44, 6054.
12. F. Wang, W. B. Tan, Y. Zhang, X. P. Fan and M. Q. Wang, Nanotech., 2006, 17, R1.
13. C. A. Mirkin, R. L. Letsinger, R. C. Mucic and J. J. Storhoff, Nature., 1996, 382, 607.
14. J. L. Seifert, R. E. Connor, S. A. Kushon, M. Wang and A. Armitage, J. Am. Chem. Soc., 1999, 121, 2987.
15. W. C. W. Chan and S. M. Nie, Science.,1998, 281, 2016.
16. Suyver, J.F., J. Grimm, J., Kramer, K.W., H.U. Gudel, H.U. Highly efficient near-infrared to visible up-conversion process in NaYF4: Er3+,Yb3+. J. Luminescence. 2005, 114, 53-59.
17. H. X. Mai, Y. W. Zhang, R. Si, Z. G. Yan, L, D, Sun, L. P. You and C. H. Yan, J. Am. Chem. Soc., 2006, 128, 6426.

18. O. Ehlert, R. Thomann, M. Darbandi and T. Nann, ACS Nano., 2008, 2, 120.

19. Mai, H., Zhang, Y., Si, R.; Yan, Z., Sun, L., You, L., Yan, C. High-quality sodium rare-earth fluoride nanocrystals: controlled synthesis and optical properties. J. Am. Chem. Soc. 2006, 128, 6426-6436.

20. Wang, F., Liu, X. Upconversion multicolor fine-tuning: visible to near-infrared emission from lanthanide-doped NaYF4 nanoparticles. J. Am. Chem. Soc. 2008, 130, 5642-5643.

21. Ehlert, O., Thomann, R., Darbandi, M., Nann, T. A four-color colloidal multiplexing nanoparticle system. ACS Nano. 2008, 2, 120-124.

22. Eustis, S., El-Sayed, M. A. Why gold nanoparticles are more precious than pretty gold: Noble metal surface plasmon resonance and its enhancement of the radiative and nonradiative properties of nanocrystals of different shapes. Chem. Soc. Rev. 2006, 35, 209-217.

23. Barnes, W. L., Dereux, A., Ebbesen, T. W. Surface plasmon subwavelength optics. Nature. 2003, 424, 824-830.

24. Tao, A., Sinsermsuksakul, P., Yang, P. Tunable plasmonic lattices of silver nanocrystals. Nat. Nanotech. 2007, 2, 435-440.

25. Daniel, M.C., Astruc, D. Gold nanoparticles: Assembly, supramolecular chemistry, quantum-size-related properties, and applications toward biology, catalysis, and nanotechnology. Chem. Rev. 2004, 104, 293-346.

26. Le, F., Brandl, D. W., Urzhumov, Y.A., Wang, H., Kundu, J., Halas, N.J., Aizpurua,

J., Nordlander, P. Metallic nanoparticle arrays: A common substrate for both surface-enhanced Raman scattering and surface-enhanced infrared absorption. ACS Nano.2008, 2, 707-718.

27. Thomas, K.G., Kamat, P.V. Chromophore-functionalized gold nanoparticles. Acc. Chem. Res. 2003, 36, 888-898.
28. Zhang, J., Fu, Y., Chowdhury, M.H., Lakowicz, J.R. Metal-enhanced single-molecule fluorescence on silver particle monomer and dimer: Coupling effect between metal particles. Nano. Lett. 2007, 7, 2101-2107.
29. Henzie, J., Lee, M.H., Odom, T.W. Multiscale patterning of plasmonic metamaterials. Nat. Nanotech. 2007, 2, 549-554.
30. Urban J.J., Talapin, D.V., Shevchenko, E.V., Kagan, C.R., Murray, C.B. Synergismin binary nanocrystal superlattices leads to enhanced p-type conductivity in self-assembled PbTe/Ag-2 Te thin films. Nat. Mat. 2007, 6, 115-121.
31. Xia, Y.N., Halas, N.J. Shape-controlled synthesis and surface plasmonic properties of metallic nanostructures. MRS Bulletin. 2005, 30, 338-344.
32. Nie, S., Emory, S.R. Probing single molecules and single nanoparticles by surface-enhanced Raman scattering. Science. 1997, 275,1102-1106.
33. Mahmoud, M.A., El-Sayed, M.A. Aggregation of gold nanoframes reduces, rather than enhances, SERS efficiency due to the trade-off of the inter- and intraparticle plasmonic fields. Nano Lett. 2009, 9, 3025-3031.
34. Campion, A., Kambhampati, P. Surface-enhanced Raman scattering. Chem. Soc. Rev.

1998, 27, 241-250.

35. Gryczynski, I., Malicka, J., Shen, Y.B., Gryczynski, Z.,Lakowicz, J.R. Multiphoton excitation of fluorescence near metallic particles: Enhanced and localized excitation. J. Phys. Chem. B. 2002, 106, 2191-2195.
36. Lakowicz, J.R. Plasmonics in biology and plasmon-controlled fluorescence. Plasmonics. 2006, 1, 5-33.
37. Pompa, P.P., Martiradonna, L,. Della, T. A., Della, S.F., Manna, L., De Vittorio, M., Calabi, F., Cingolani, R., Rinaldi, R. Metal-enhanced fluorescence of colloidal nanocrystals with nanoscale control. Nature Nanotech. 2006, 1, 126-130.
38. Shevchenko, E. V., Ringler, M., Schwemer, A., Talapin, D.V., Klar, T. A., Rogach, A. L., Feldmann, J., Alivisatos, A. P. Self-assembled binary superlattices of CdSe and Au nanocrystals and their fluorescence properties. J. Am. Chem. Soc. 2008, 130, 3274 – 3275.
39. Chen, Y., Munechika, K., Ginger, D.S. Dependence of fluorescence intensity on the spectral overlap between fluorophores and plasmon resonant single silver nanoparticles. Nano Lett. 2007, 7, 690-696.

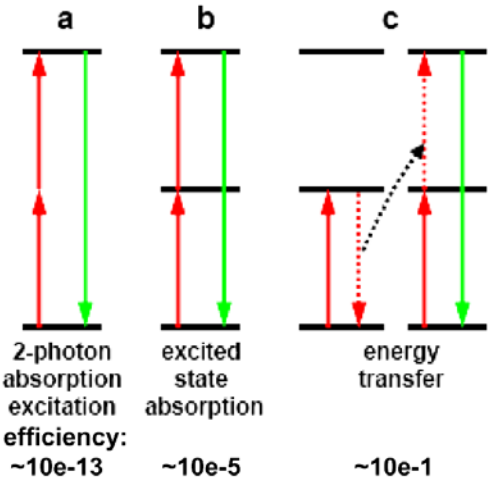

Figure 1-1. Three schemes for energy up-conversion process and the corresponding approximate efficiency.

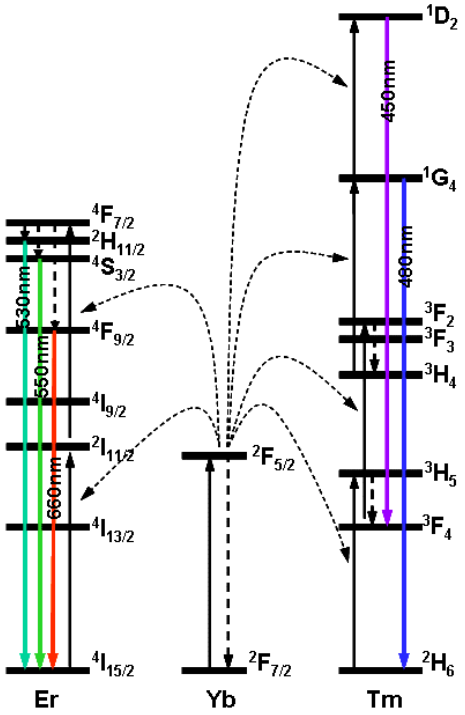

Figure 1-2. Energy levels of rare earth elements and the energy transfer process. Energy levels of Yb mediated upconversion process in Er where the emission can be green or red, and in Tm where emission can be violet or blue depending on exact energy levels involved.

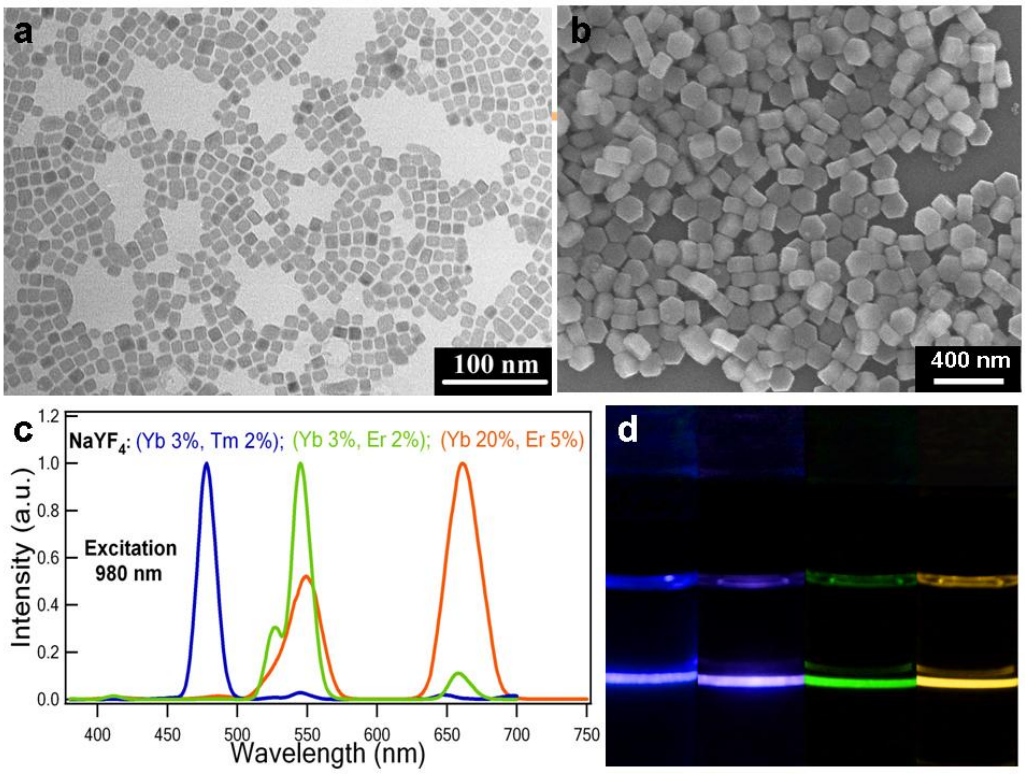

Figure 1-3. Preliminary results on upconversion nanoparticles. (a,b) TEM and SEM image of cubic and hexagonal Yb-Tm co-doped NaYF4 nanoparticles with the size range from 20-200 nm. (c) Energy upconversion spectra observed in Yb-Tm and Yb-Er co-doped NaYF4 nanoparticles, where the emission can be blue, green or red depending on exact doping material and doping ratio. With this type of materials, the emission color can be readily tuned by varying the doping elements and/or concentration. (d) Photographs of fluorescence from Yb-Tm and Yb-Er co-doped NaYF4 nanoparticles when excited with 980 nm diode laser. The violet and blue emission is from $NaYF_4$ (Yb-Tm) nanoparticles; the green and yellow (mix of green and red) emission is from $NaYF_4$ (Yb-Er) nanoparticles.

Chapter 2 Composition Tuning for Upconversion Nanocrystals

2.1 Introduction

Trivalent rare earth element (Re^{3+}) doped materials are among the most promising materials for energy upconversion because they have multiple long-lived excited states and can exhibit highly efficient energy transfer processes that are responsible for upconversion emission under certain conditions.[1-4] Here we focus our efforts on Yb-Tm doped systems that can emit violet (452 nm) or blue (476 nm) light, aiming to rationally tune the relative emission intensity at different speactral peaks through the controlling of the exact doping concentration. The ability to achieve this shorter wavelength emission through an upconversion process is of significance for activating certain chemical or biological processes. For example, the 476 nm light can be used to excite channelrhodopsins, which are a subfamily of opsin proteins that function as light-gated ion channels in neural cells.[5] Therefore, it is important that the emission wavelength can be tuned by introducing different dopants or doping ratios. By varing the the exact doping concentration during the chemical synthesis process, we show the overall and relative emission intensity of the selected spectral peaks can be readily tuned.

2.2 Experiment

2.2.1 Synthesis

$NaYF_4$ can adopt either a cubic or hexagonal structure.[3,6,7] It is well known that the hexagonal structure is the most efficient matrix for upconversion phosphors.[8-10] The synthesis of $NaYF_4$ hexplate nanocrystals (NCs) achieved through a solution chemical approach at high temperature, similar to previous reports.[11-13] Specifically, the synthesis was carried out with standard oxygen-free procedures and all chemicals were purchased from Sigma-Aldrich and used without further purification. In a typical procedure, a certain amount of yttrium(III) oxide (Y_2O_3, 99.99%), ytterbium(III) oxide (Yb_2O_3, 99.9%) and thulium(III) oxide (Tm_2O_3, 99.9%) (1.25 mmol in all with the relative ratio depending on the exact doping concentration) were dissolved in 5 mL trifluoroacetic acid (TFA, 99%) in a 100 mL three-necked flask. The slurry was then heated to 120 ^oC with vigorous magnetic stirring under vacuum for 30 minutes to remove water and excessive TFA. Next, 2.5 mmol sodium trifluoroacetate ($NaCOOCF_3$, 98%) was added, along with 7.5 mL of oleic acid (OA, 90%) and 7.5 mL of 1-octadecene (ODE, 90%) at 100oC. Afterwards, the solution was heated to 330 ^oC with a rate of 30 ^oC min-1 and maintained at 330 ^oC for 60 minutes to obtain the NCs.

2.2.2 Characterization

The microstructures, morphologies the $NaYF_4$:Yb/Tm NCs were characterized by a JEOL 6700 FEG scanning electron microscope (SEM). The microstructures and lattice images of $NaYF_4$:Yb/Tm NCs were observed by an FEI CM120 transmission electron microscope (TEM) and an FEI Titan high-resolution transmission electron microscope

(HRTEM). The composition of the NCs was characterized using energy-dispersive X-ray spectroscopy (EDX). Room temperature photoluminescence spectra were collected on a Spec-10® system from Princeton Instruments including a liquid nitrogen cooled CCD camera (Spectra Pro® 2300i, Model: 7509-0001). Confocal photoluminescence images were taken on a Leica TCS-SP2 AOBS inverted Confocal and Multiphoton Microscope (Mannheim, Germany) equipped with a Spectra-Physics MaiTai picosecond pulsed infrared laser (Mountain View, CA) set at 980 nm for infrared excitation.

The SEM and TEM image shows that the $NaYb_{0.99}Tm_{0.01}F_4$ NCs have a hexagonal plate structure with nearly mono-dispersed sizes (Fig. 2-1 a,b). The diagonal length of the hexagonal plate is about 180 nm with a thickness of 50 nm. The well-defined hexagonal morphology of the NCs suggests that they are single crystals. Indeed, the HRTEM and SAED images confirmed that the as-prepared NCs are single crystals with a hexagonal phase. The lattice spacing of 5.13 Å in HRTEM image corresponds to (100) lattice planes (Fig. 2-1c and inset).

As the upconversion emission wavelength and efficiency can be greatly affected by the exact doping concentrations. We have carried out systematic studies to control the rare earth element doping concentration in these NCs. Importantly, our studies show that doping concentration in the final NC product is directly correlated to the initial reactant ratio before synthesis. For example, we have prepared a series of $NaY_{0.8-x}Yb_{0.2}Tm_xF_4$ and $NaYb_{1-x}Tm_xF_4$ NCs with variable Tm^{3+} ion concentrations. The plot of the Tm^{3+} concentration in the NCs vs. the starting reactant ratio shows a clear linear relation with a

slope close to one (Fig. 2-2). These studies demonstrate that all the rare earth elements can be effectively incorporated into the final NCs with our synthetic conditions. Therefore, the Re^{3+} doping concentration can be readily controlled by varying the initial reactant ratio. The size, morphology and dispersity of the NCs of variable compositions remained similar to what have been shown in Figure 2-1.

2.3 Results and discussion

2.3.1 Energy transfer process

In Re^{3+} doped materials, the energy transfer process between adjacent ions is the primary reason responsible for the upconversion emission. Therefore, a close match between different transition levels of the rare earth ions can critically impact the probability of energy transfer process and the efficiency of the upconversion process. In the Yb-Tm co-doped materials, the infrared radiation can be efficiently converted into blue emission by a three-photon process or violet emission by a four-photon upconversion process due to the existence of multiple energy resonances in the system (Fig. 2-3). One energy transfer step from Yb^{3+} ion to Tm^{3+} ion populates the $^3H_5$ level of Tm^{3+} from $^3H_6$. The $^3H_5$ decays rapidly to the $^3F_4$ level. The second energy transfer step raises the Tm^{3+} ion from $^3F_4$ to $^3F_2$ that quickly decays to $^3H_4$. Subsequently, the third transfer step raises the Tm^{3+} ion from $^3H_4$ to $^1G_4$ that can yield a blue emission upon radiative relaxation back to $^3H_6$. A fourth energy transfer step from Yb^{3+} ion to Tm^{3+} ion may also take place to populate the Tm^{3+} ion from $^1G_4$ to $^1D_2$, which is however usually

less efficient due to relative large energy mismatch. An alternative way to populate $^1D_2$ is through cross relaxation between adjacent Tm^{3+} ions with three possible routes: $^3F_2 \rightarrow {}^3H_6$ and $^3H_4 \rightarrow {}^1D_2$; $^1G_4 \rightarrow {}^3F_4$ and $^3H_4 \rightarrow {}^1D_2$; and $^1G_4 \rightarrow {}^1D_2$ and $^3H_4 \rightarrow {}^3F_4$.[14] The relaxation of $^1D_2$ to $^3F_4$ leads to a violet emission.

The upconversion emission of the NCs were characterized in chloroform solution with fixed amount of NCs (typically 1 wt %) of variable Tm^{3+} concentration under 980 nm diode laser excitation with a total power of 38 mW.

2.3.2 Composition tuning in $NaY_{0.8-x}Yb_{0.2}Tm_xF_4$ system

Figure 2-4a shows the emission spectra of $NaY_{0.8-x}Yb_{0.2}Tm_xF_4$ nanoparticles at different doping concentrations of Tm^{3+} ions. The two strongest peaks occur at 452 nm (violet) and 476 nm (blue), corresponding to relaxation of $^1D_2 \rightarrow {}^3F_4$ and $^1G_4 \rightarrow {}^3H_6$, respectively. The intensity increases slightly when the Tm^{3+} concentration is increased from 0.05 to 0.2 mol % and then decreases with further increase of Tm^{3+} concentration. It is reasonable to assume that if the Tm^{3+} ion concentration is too low, there will not be enough Tm^{3+} ion to be populated or excited.[2] At this point, the emission intensity increases with increasing number of Tm^{3+} ions in the system. On the other hand, further increase the Tm^{3+} concentration beyond a certain threshold can lead to a decrease in the emission intensity. This is because a cross-relaxation mechanism exists between Tm^{3+} ions that can lead to a self-quenching effect: the increase of the Tm^{3+} concentration leads to a decrease in the distance between adjacent Tm^{3+} ions and an increase in the

probability of cross-relaxation that reduces radiative relaxation, and thus suppresses the upconversion emission in high Tm^{3+} ion concentrated samples.[15] Plotting the upconversion emission intensity normalized by the number of Tm^{3+} ions as a function of Tm^{3+} concentration, a monotonic decrease in intensity could be observed (Fig. 2-4c), suggesting that the cross-relaxation between neighboring Tm^{3+} ions exists in all samples include the very low-dope samples.

Figure 2-4a also shows that the preferred emission wavelength also changes from blue to violet with increasing the Tm^{3+} concentration. The digital camera images of NCs fluorescence clearly show different colors (from blue to violet) for the samples with increasing Tm^{3+} ion doping concentration (Fig. 2-4b). Plotting the ratio of violet vs. blue emission ($f_{v/b}$) shows a monotonic increase with the increasing Tm^{3+} ion concentration (Fig. 2-4d). This color change as a function of Tm^{3+} ion concentration may be attributed to possible cross-relaxation processes: $^1G_4 \rightarrow {}^3F_4$ and $^3H_4 \rightarrow {}^1D_2$; and $^1G_4 \rightarrow {}^1D_2$ and $^3H_4 \rightarrow {}^3F_4$. These cross relaxation processes decrease $^1G_4$ population and increase $^1D_2$ population. Therefore, with increasing Tm^{3+} ion concentration and increasing probability of cross-relaxation, one would expect to see relatively more violet emission originated from $^1D_2$ state and less blue emission originated from $^1G_4$ state, resulting in an increase in violet/blue ratio ($f_{v/b}$) with the increase of Tm^{3+} concentration.

2.3.3 Composition tuning in $NaYb_{1-x}Tm_xF_4$ system

Additionally, we have further explored a simpler $NaYbF_4$:Tm system, using

$NaYbF_4$ as the matrix and Tm as the dopant, and investigated the emission intensity vs. doping concentration. Figure 2-5a shows the emission spectra of a series of $NaYbF_4$:Tm NCs with variable Tm^{3+} concentration. Interestingly, only one dominant emission peak at 452 nm can be seen in this system. A maximum violet over blue emission ratio of 5.5 is observed. Removing Y^{3+} ion away from the system increases the overall concentration of both Yb^{3+} and Tm^{3+} ions, which can facilitate cross-relaxation between Tm^{3+} ions to increase violet emission and decrease blue emission. Additionally, cross-relaxation between Tm^{3+} ions to Yb^{3+} ions can also take place, which reduces the population in $^1G_4$ state in a more significant way than $^1D_2$ state,[16] and thus significantly suppress 476 nm emission from $^1G_4$ state, leaving the 452 nm (violet) emission from the $^1D_2$ state only dominant peak here.

The spectra in Fig. 5a also show that the best intensity is observed in sample with composition of $NaYb_{0.99}Tm_{0.01}F_4$, either decrease or increase in the Tm^{3+} concentration will result in a decrease in overall upconversion intensity. Normalizing the emission intensity by the number of Tm^{3+} ions, a monotonic decrease of the emission intensity vs. doping concentration could be easily observed (Fig. 2-5b), which is consistent with the result shown in Fig. 2-4c, suggesting the cross-relaxation between adjacent Tm^{3+} ions is primarily responsible for the self-quenching and the decrease of emission intensity at high Tm^{3+} concentration.

2.3.4 Confocal study

Lastly, we have also used confocal microscope to investigate the upconversion emission from individual NCs. To this end, the NCs were first spin-coated onto a glass slide. The reflection image of the NCs on glass slide shows well separated NCs or NC clusters (Fig. 2-6a). SEM image of a similar sample prepared on silicon wafer further shows the NCs are either single NCs or a few NC clusters (inset, Fig. 2-6a). Importantly, confocal photoluminescence image (Fig. 2-6b) clearly shows strong emission from the NCs when excited with 980 nm laser, with each bright spot in the image corresponding to emission from one or a few NCs. These studies clearly show that upconversion emission from individual NCs can be readily visualized by a confocal microscope, which is significance for exploring them as fluorescence tags for biomedical imaging.

2.4 Summary

In summary, we successfully prepared $NaYF_4$:Yb/Tm hexagonal plate NCs with precisely controlled composition/doping concentration by varing the doping concentration when synthesizing the NCs. Photoluminescence studies show strong upconversion emission in blue and violet region from the NCs when excited with 980 nm light. Importantly, the overall emission intensity and relative ratio of these two emission colors can be readily tuned by varying the exact Re^{3+} doping concentration. These studies demonstrate a rational approach to tune the upconversion emission from rare earth element doped nanomaterials, and can impact broadly from energy harvesting, energy conversion to biomedical imaging and therapeutics.

References

1. Auzel, F., Upconversion and anti-stokes processes with f and d ions in solids. *Chemical Reviews* 104 (1), 139-173 (2004).
2. D. R. Gamelin and H. U. Gudel, Top. Curr. Chem., 2001, 214, 1.
3. H. X. Mai, Y. W. Zhang, L. D. Sun and C. H. Yan, J. Phys. Chem. C., 2007, 111, 13730.
4. H. X. Mai, Y. W. Zhang, L. D. Sun and C. H. Yan, J. Phys. Chem. C., 2007, 111, 13721.
5. G. Nagel, T. Szellas, W. Huhn, S. Kateriya, N. Adeishvili, P. Berthold, D. Ollig, P. Hegemann and E. Bamberg , Proc. Natl. Acct. Sci., 2003, 100, 13940.
6. H. X. Mai, Y. W. Zhang, R. Si, Z. G. Yan, L, D, Sun, L. P. You and C. H. Yan, J. Am. Chem. Soc., 2006, 128, 6426.
7. L. Y. Wang and Y. D. Li, Chem. Master., 2007, 19, 727.
8. L. F. Liang, H. Wu, H. L. Hu, M. M. Wu and Q. Su, J. Alloys Compd., 2004, 368, 94.
9. A. Aebischer, M. Hostettler, J. Hause, K. Kramer, T. Weber, H.U. Gudel and H. B. Buergi, Angew. Chem. Int. Ed., 2006, 45, 2802.
10. K. W. Kramer, D. Biner, G. Frei, H. U. Gudel, M. P. Hehlen and S. R. Luthi, Chem. Mater., 2004, 16, 1244.
11. O. Ehlert, R. Thomann, M. Darbandi, T. Nann, ACS Nano 2008, 2, 120.
12. J. C. Boyer, L. A. Cuccia and J. A. Capobianco, Nano Lett. 2007, 7, 847.

13. H. Zhang, Y. Li, I. A. Ivanov, Y. Qu, Y. Huang, and X. Duan, Angew Chemie Intl. Ed. 2010, 16, 2865.
14. G. Wang, W. Qin, L. Wang, G. Wei, P. Zhu and R. Kim, Optics Exp., 2008, 16 ,11907.
15. F. Wang and X. G. Liu, J. Am. Chem. Soc. 2008, 130, 5642.
16. W. Ryba-Romanowski, S. Golab, G. Dominiak-Dzik, M. Zelechower and J. Gabrys-Pisarska, J. Alloys Compd., 2001, 325, 215.

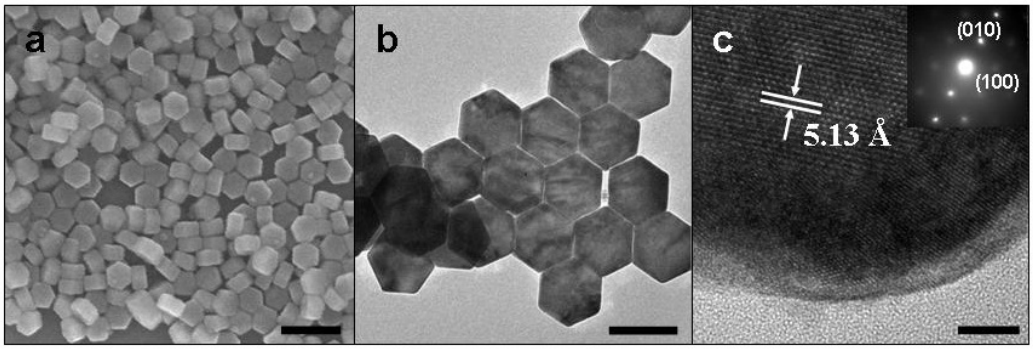

Figure 2-1 (a) SEM, (b) TEM, (c and inset) HRTEM and SAED images of $NaYbF_4$:Tm NPs with uniform hexagonal shape (the scale bars correspond to 400 nm, 200 nm and 5 nm, respectively).

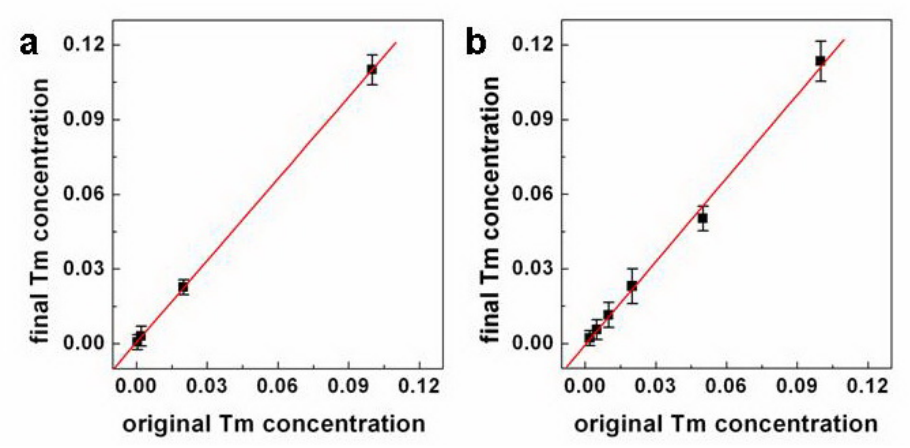

Figure 2-2 Diagram of final Tm^{3+} concentration versus original Tm^{3+} concentration in (a) $NaY_{0.8-x}Yb_{0.2}Tm_xF_4$ NCs and (b) $NaYb_{1-x}Tm_xF_4$ NCs.

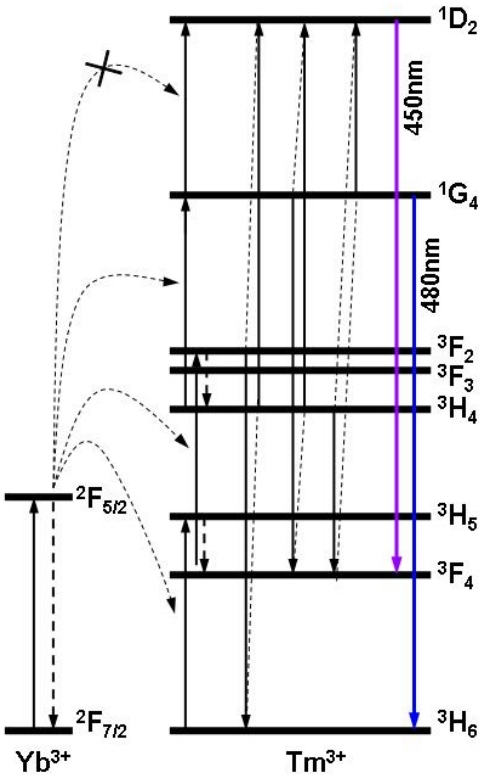

Figure 2-3 Schematic illustration of the energy levels invovled in the upconversion process of Tm^{3+} with Yb^{3+} as the promoter for $NaYF_4$:Yb,Tm NCs.

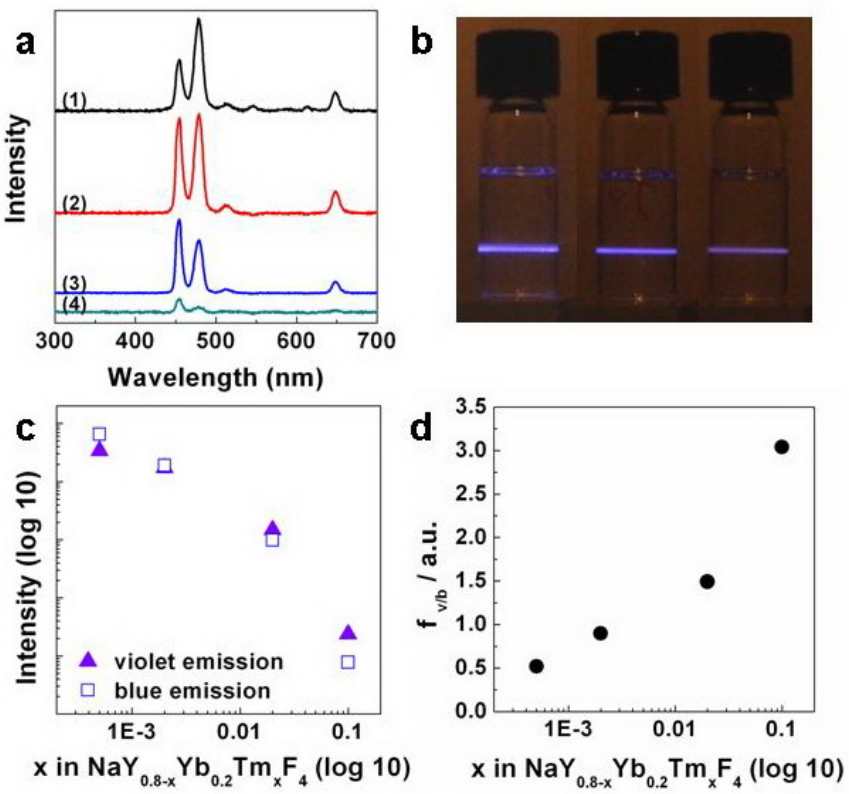

Figure 2-4 (a) Upconversion emission spectra of $NaY_{0.8-x}Yb_{0.2}Tm_xF_4$ NCs with different Tm^{3+} concentrations, x = 0.0005, 0.002, 0.02, 0.1, for (1), (2), (3), (4) respectively. (b) Digital camera pictures of $NaY_{0.78}Yb_{0.2}Tm_{0.02}F_4$, $NaY_{0.798}Yb_{0.2}Tm_{0.002}F_4$ and $NaY_{0.7995}Yb_{0.2}Tm_{0.0005}F_4$ samples under 980 nm excitation. (c) Upconversion emission intensity (normalized by Tm^{3+} ion concentration) versus doping concentration of Tm^{3+} in $NaY_{0.8-x}Yb_{0.2}Tm_xF_4$ NCs. (d) Diagram of violet to blue emission ($f_{v/b}$) ratio versus Tm^{3+} doping concentration in $NaY_{0.8-x}Yb_{0.2}Tm_xF_4$ NCs.

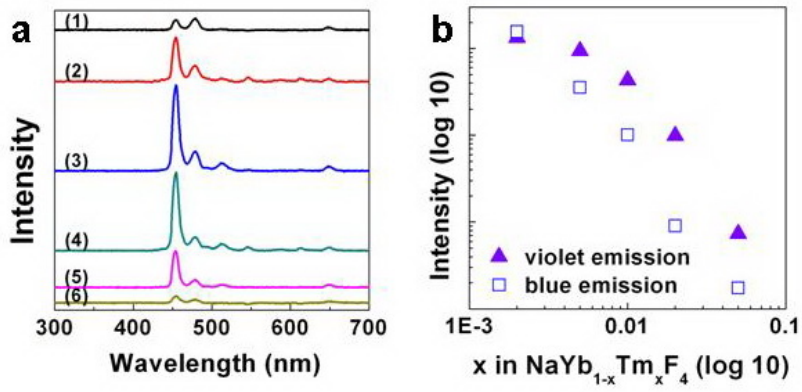

Figure 2-5 (a) Upconversion emission spectra of $NaYb_{1-x}Tm_xF_4$ NCs with different Tm^{3+} concentrations, x = 0.002, 0.005, 0.01, 0.02, 0.05, 0.1, for (1), (2), (3), (4), (5), (6) respectively. (b) Tm^{3+} normalized upconversion emission intensity versus doping concentration of Tm^{3+} in $NaYb_{1-x}Tm_xF_4$.

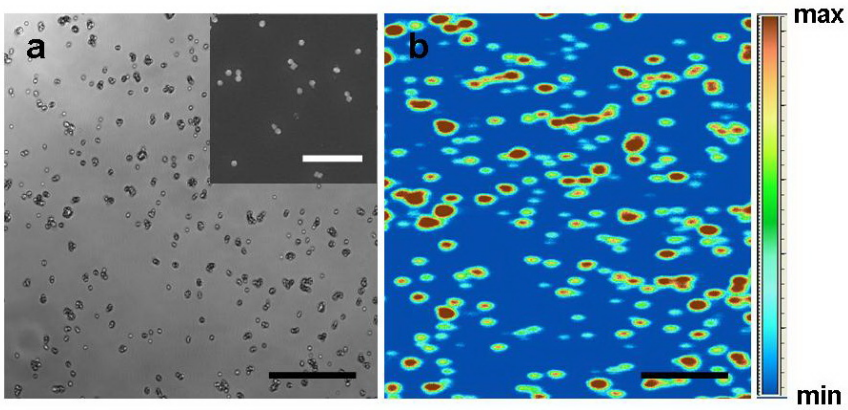

Figure 2-6 (a) Reflection image of NCs on glass substrate. (inset) SEM image of a similar sample prepared on silicon wafer. (b) Confocal photoluminescence image of the upconversion nanocrystals shown in (a). (Scale Bar: 25 μm for (a) and (b), and 5μm for the inset).

Chapter 3 Plasmonic Modulation for Upconversion Fluorescence using Gold Nanoparticles or Nanoshells

3.1 Introduction

The studies show that gold nanoparticles (NPs) can be attached onto the upconversion NCs with variable density, which can further function as the nucleation seeds for the growth of continuous gold nanoshells. The attachment of gold NPs is found to significantly enhance the upconversion emission. Spectroscopic studies suggest that this enhancement exhibit strong spectral dependence, and may be largely attributed to surface plasmon coupled emission which increases the radiative decay rate and the emission efficiency. On the contrary, gold nanoshell can greatly suppress the emission possibly due to the strong scattering of excitation irradiation. These findings open a new pathway to rationally modulate the upconversion emission, and can broadly impact in areas including biomedical imaging, sensing and therapeutics, as well as enable new opportunities for energy harvesting and conversion.

Surface plasmon resonance (SPR) is the collective electron cloud oscillation on a metal surface or NP caused by its interaction with incident light.[1,2] This leads to a number of interesting optical events such as the absorption and scattering of photons of certain wavelength and is responsible for the wide range of colors observed in colloid metal nanoparticles.[3,4] Additionally, the large local electrical fields generated by SPR in the vicinity of the NPs can significantly modify spectroscopic properties of neighbouring fluorophores.[5-7] SPR is largely responsible for surface enhanced Raman spectroscopy

(SERS) with an enhancement factor of up to 10^{14}-10^{15}, allowing the technique to be sensitive enough for single molecule detection.[8-10] Recently, gold and silver NPs or islands have been explored to modulate fluorescent emission from various nanostructures such as semiconductor quantum dots or fluorescent molecules.[11-13]

3.2 Experiment

3.2.1 Synthesis and ligand exchange

Our $NaYF_4$:Yb/Tm NCs were synthesized by thermal decomposition of rare-earth/sodium trifluoroacetate precursors in oleic acid and octadecene in a similar process in Chapter 2.2.1.[14] The as-synthesized NCs are terminated with oleic acid ligands and are hydrophobic. The attachment of gold NPs and the growth of gold nanoshells are typically carried out in aqueous solution, requiring the dispersion of the NCs into water. To this end, two steps of surface modification have been performed for gold seed attachment and gold shell growth (Scheme 3-1). First, a ligand exchange process was done by using poly (acrylic acid) (PAA) as a multidentate ligand which displaces the original hydrophobic ones on the NC surface. The resulting PAA coated NCs are typically negatively charged. To facilitate the subsequent attachment of the negatively charged gold NPs, an additional layer of poly (allylamine hydrochloride) (PAH) is coated onto the NC surface to render them positively charged. To ensure each surface modification process was achieved successfully, Fourier Transform Infrared (FTIR) spectra were taken to

confirm the additional existence of the –COOH or $–NH_2$ groups (Fig 3-1). To attach the gold NPs onto the NC surface, negatively charged gold NPs were first prepared separately and then mixed with the upconversion NC aqueous solution in proper ratio and allowed to age for a controlled time. Gold shell growth is then carried out by introducing additional gold precursor and reductant into the upconversion NC solution.

In a typical procedure, 0.9 mmol of yttrium(III) oxide (Y_2O_3, 99.99%), 0.18 mmol of ytterbium(III) oxide (Yb_2O_3, 99.9%) and 0.036 mmol of thulium(III) oxide (Tm_2O_3, 99.9%) were dissolved in 5 mL trifluoroacetic acid (TFA, 99%) in a 100 mL three-necked flask. The slurry was then heated to 80 ^oC with vigorous magnetic stirring under vacuum for 30 minutes to remove water and excessive TFA. Next, 2.5 mmol sodium trifluoroacetate ($NaCOOCF_3$, 98%) was added, along with 7.5 mL of oleic acid (OA, 90%) and 7.5 mL of 1-octadecene (ODE, 90%) at 100^oC. Afterwards, the solution was heated to 330 ^oC with a rate of 30 ^oC min^{-1} and maintained at 330 ^oC for 60 minutes to obtain the NCs.

For the surface modification: first, a ligand exchange process was done using poly (acrylic acid) (PAA, M_w = 1,800) as a multidentate ligand which displaces the original hydrophobic ones on the NC surface: by mixing 10 ml PAA solution in ethanol (~1 wt %) and 5 mL of NCs dispersion in chloroform (~1 wt %) together with overnight stirring, the solution was then centrifuged at 14,000 rpm for 30 min. After being washed 3 times with ethanol, the particles can be re-dispersed in water well. A similar procedure for additional layer of poly(allylamine hydrochloride) (PAH, M_w = 56,000) could be easily achieved

except for that the process was conducted in deionized (DI) water.

For the attachment of the gold NPs: gold nanoseed solution was first prepared as follows: 12 μL of 80 % tetrakis-hydroxymethyl-phosphonium chloride (THPC) and 0.25 mL of 2 M NaOH was added to 45 mL of DI water. The mixture was stirred vigorously for 5 min before 2.0 mL of 1% $HAuCl_4$ was quickly introduced in one shot. An immediate color change to dark brown was observed. This solution was stored in a lightproof container with stirring overnight. By combining 1 mL of PAH coated upconversion NC solution with 10 mL of gold seed solution, the gold NPs could attach onto the upconversion NC surface after 6 hours for curing.

For the growth of the gold nanoshells: the aged gold solution was first prepared by dissolving 25 mg of potassium carbonate in 100 mL DI water. After 10 min, 1.5 mL of 1% $HAuCl_4$ was added and the solution turned colorless over the course of 10 min. This solution was aged for one day. While stirring vigorously, 1 mL of solution of upconversion NCs (with gold nanoseed attached) was added to 10 mL of the aged gold solution. A reducing agent formaldehyde (29%, 50 L) was then introduced very slowly. Upon mixing, the color of the mixture immediately changed from colorless to brownish-blue and a black precipitate could be observed quickly.

3.2.2 Characterization

The microstructures, morphologies and composition of the $NaYF_4$:Yb/Tm NCs

and gold seed NPs were characterized by an FEI CM120 transmission electron microscope (TEM) and an FEI Titan high-resolution transmission electron microscope (HRTEM). Room temperature fluorescence spectra were collected on a Spec-10® system from Princeton Instruments including a liquid-nitrogen cooled CCD camera. Confocal fluorescence images were taken on a Leica TCS-SP2 AOBS inverted Confocal and Multiphoton Microscope (Mannheim, Germany) equipped with a Spectra-Physics MaiTai picosecond pulsed infrared laser (Mountain View, CA) set at 980 nm for infrared excitation. The UV-Vis spectra were taken by a Beckman-Coulter spectrophotometer (DU® 800) and the Fourier Transform Infrared (FTIR) spectra were taken by a JASCO® FT/IR-420 spectrometer.

The microstructures, morphologies and composition of the $NaYF_4$:Yb/Tm NCs were characterized by a transmission electron microscope (TEM). The as-prepared upconversion NCs typically have a hexagonal structure with uniform size around 180 nm (Fig. 3-2a). The relatively uniform contrast in TEM image suggests the NCs are single crystals, which can be confirmed by high resolution TEM images and electron diffraction patterns (Fig. 3-3). With the attachment of gold NPs, increasing number of darker specks can be observed, in which each dark speck corresponds to a gold NP on the upconversion NC surface (Fig. 3-2 b,c). During the Au shell growth stage, these Au NPs function as the seeds for the nucleation of gold on the upconversion NC surface. As the reaction proceeds, the size of the gold NPs grows rather quickly and eventually merges together to form a continuous shell (Fig. 3-2 d-f).

3.3 Results and discussion

3.3.1 Spectral study

The emission spectra of the upconversion NCs during the seeding stage show a significant increase in emission intensity with increasing the number of attached Au NPs, and an enhancement factor of more than 2.5 was achieved (Fig. 3-4a). On the other hand, during the gold shell growth stage, the evolution of emission spectra show that the emission intensity decreases substantially as the shell forms (Fig. 3-4b). These studies clearly demonstrate that the attachment of gold NPs on upconversion NC surface can enhance the upconversion emission, while the formation of the continuous gold shell can quench the emission. Additionally, it is interesting to note that the emission enhancement by Au NPs is highly wavelength dependent, with the enhancement factors in violet/blue region much larger than that in the red region (Fig. 3-4c). Specifically, more than 150% increase in emission intensity is observed at 452 nm and 476 nm, while only ~50% increase is seen at 647 nm. On the other hand, the quenching of the emission by the gold shell has much less dependence on the wavelength, with the quenching factors remaining roughly the same for all emission peaks. (Fig. 3-4d)

3.3.2 Confocal study

To confirm this modulation in emission intensity is indeed originated from individual upconversion NCs rather than any other complex effect in solution, we used

confocal microscope to investigate the upconversion emission from individual NCs. To this end, the NCs were first spin-coated onto a glass slide, and then cured in gold seed solution for Au NP attachment, and the upconversion emission was monitored with increasing curing time. To ensure that we compared the emission from the exact same location, we have used lithography to create alignment markers on the glass slide. The reflection image of the NCs on the glass slide shows well separated NCs or NC clusters (Fig. 3-5a). The SEM image of a similar sample prepared on silicon wafer further shows the NCs are either single NCs or a-few-NC clusters (Fig. 3-5b). Confocal fluorescence image (Fig. 3-5c-e) of the same sample at the same area shown in Figure 3-5a clearly shows strong upconversion emission from the NCs when excited with 980 nm laser, with each bright spot in the image corresponding to emission from one or a few NCs. Importantly, the confocal images clearly show that the upconversion emission from individual NCs can be significantly enhanced with increasing curing time in gold seed solution, demonstrating that the enhancement can be attributed to individual NCs upon the attachment of gold NPs. Quantitative analysis of the confocal images shows that an intensity enhancement factor of c.a. 2.6 can be achieved (Fig. 3-5f), consistent with the results in Figure 2a.

3.3.3 Enhancement effect discussion

The observed enhancement in the upconversion emission is in stark contrast to the usual perception that the presence of metal in close proximity can lead to a quench in the fluorescence emission. We suggest the enhancement effect by the gold NPs may be attributed to at least two possible reasons: (1) an increase of excitation rate by local field enhancement (LFE): an enhancement of effective excitation flux caused by local field enhancement associated with plasmonic resonance; (2) an increase of emission rate by surface plasmon coupled emission (SPCE): an enhancement of emission efficiency due to the coupling of the upconversion emission with the NP plasmonic resonance which will effectively increase both the non-radiative and radiative decay rate. SPCE can occur when the emission band of the fluorophore overlaps with the plasmon resonance frequency of the metal nanostructures.[11] Importantly, both of these factors have been used to account for the metal-enhanced fluorescence (MEF) in quantum dot or fluorescent molecules.[12,13]

3.3.4 UV-Vis study

To determine which factor played the primary role in the enhancement of upconversion emission by Au NPs, we have characterized the plasmon resonance properties of NC-NP conjugates using UV-Vis absorption spectra. Importantly, UV-Vis spectra of the gold NPs and NC-NP conjugates show a resonance peak around 510 nm (Fig. 3-6a), consistent with the plasmon resonance frequencies observed in similar gold

NPs.[15,16] Slight red-shift is observed with increasing density of gold NPs on NC surface, which is also consistent with previous observations that the SPR peak would red shift with the aggregation of gold NPs.[17-19] This plasmonic resonance frequency of gold NPs overlaps well with the two major emission peaks in the upconversion NCs (452 nm and 478 nm). Therefore, the gold NP SPR can effectively couple with the upconversion emission and can thus increase the radiative decay rate, emission efficiency and intensity. With a better plasmonic coupling near the plasmon resonance frequency, this SPCE also explains well why a larger enhancement factor is observed in violet/blue emission than in red emission (Fig. 3-4a,c). On the other hand, when a continuous gold shell is formed, the SPR peak is shifted to near-infrared region (Fig. 3-6b), which is highly dependent on the thickness and geometry of the gold shell.[20-22] This shift of SPR reduces the SPCE and significantly increases the scattering of excitation light at 980 nm, and thus reduces the effective excitation flux, leading to a quench of the upconversion emission.

3.4 Summary

In summary, we have reported a new approach to modulate upconversion emission through plasmonic interaction between the upconversion NCs and gold nanostructures. The attachment of the gold NPs onto upconversion NCs can more than double the upconversion emission intensity. This enhancement can be at least partly attributed to SPCE that can increase the radiative decay rate and emission efficiency,

although further study will be necessary to fully elucidate the exact underlying mechanism. The formation of gold shell can significantly suppress the emission due to significant scattering of excitation irradiation. These findings open a general pathway to rationally modulate the upconversion emission, and can broadly impact areas including biomedical imaging, therapeutics and energy conversion.

References

1. S. Eustis, M. A. El-Sayed, Chem. Soc. Rev. 2006, 35, 209.
2. W. L. Barnes, A. Dereux, T. W. Ebbesen, Nature 2003, 424, 824.
3. A. Tao, P. Sinsermsuksakul, P. Yang, Nat. Nanotechnol. 2007, 2, 435.
4. M. C. Daniel, D. Astruc, Chem. Rev. 2004, 104, 293.
5. F. Le, D.W. Brandl, Y.A. Urzhumov, H. Wang, J. Kundu, N.J. Halas, J. Aizpurua, P. Nordlander, ACS Nano. 2008, 2, 707.
6. K. G. Thomas, P. V. Kamat, Acc. Chem. Res. 2003, 36, 888.
7. J. Zhang, Y. Fu, M. H. Chowdhury, J. R. Lakowicz, Nano. Lett., 2007, 7, 2101.
8. S. Nie, S. R. Emory, Science. 1997, 275, 1102.
9. M. A. Mahmoud, M. A. El-Sayed, Nano Lett. 2009, 9, 3025.
10. A. Campion, P. Kambhampati, Chem. Soc. Rev. 1998, 27, 241.
11. J. R. Lakowicz, Plasmonics 2006, 1, 5.
12. I. Gryczynski, J. Malicka, Y. B. Shen, Z. Gryczynski, J. R. Lakowicz, J. Phys. Chem.

B 2002, 106, 2191.

13. J. R. Lakowicz, Anal. Biochem. 2001, 298, 1.

14. J.C. Boyer, L. A. Cuccia, J. A. Capobianco, Nano Lett., 2007, 7, 847

15. S. Link, M. A. El-Sayed, J. Phys. Chem. B 1999, 103, 4212.

16. B. J. Messinger, K. Ulrich von Raben, R. K. Chang, P. W. Barber, Phys. Rev. B 1981, 24, 649.

17. S. K. Eah, H. M. Jaeger, N. F. Scherer, X. M. Lin, G. P. Wiederrecht, Chem. Phys. Lett. 2004, 386, 390.

18. M. J. Feldstein, C. D. Keating, Y. Liau, M. J. Natan, N. F. Scherer, J. Am. Chem. Soc. 1997, 119, 6638.

19. J. W. Bai, S. X. Huang, L. Y. Wang, Y Chen, Y Huang, J. Mater. Chem., 2009, 19, 921

20. S. J. Oldenburg, R. D. Averitt, S. L. Westcott, N. J. Halas, Chem. Phys. Lett. 1998, 288, 243.

21. H. Wang, G. P. Goodrich, F. Tam, C. Oubre, P. Nordlander, N. J. Halas, J. Phys. Chem. B 2005, 109, 11083.

22. L. Y. Wang, J. W. Bai, Y. J. Li, Y. Huang, Angew. Chem. Int. Ed. 2008, 47, 2439

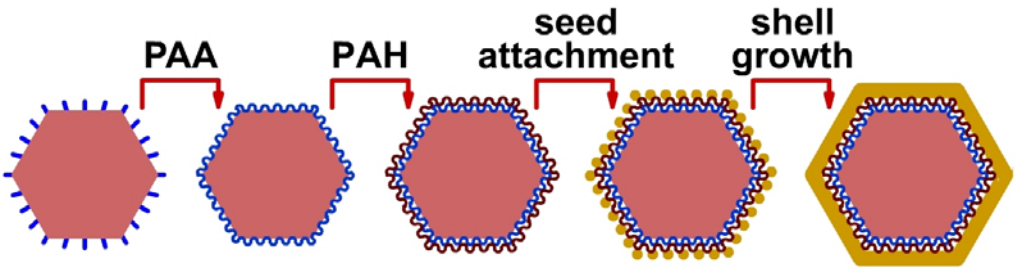

Schemetic 3-1. Schematic illustration of surface functionalization, gold NP attachment, and gold nanoshell growth on the upconversion NCs.

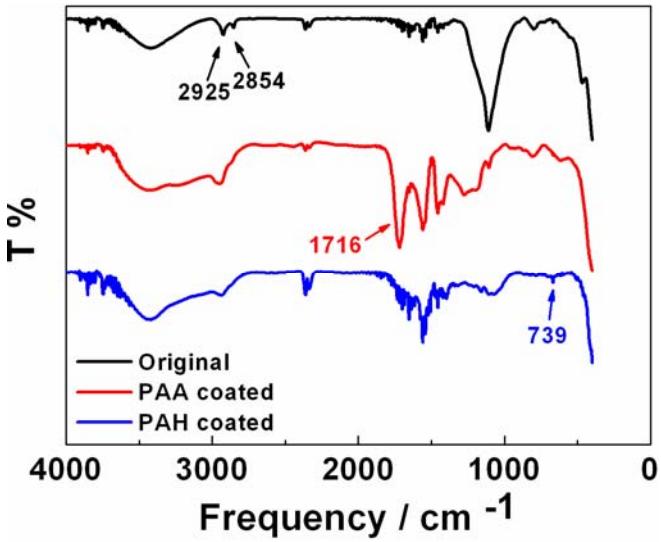

Figure 3-1 FTIR spectra of upconversion NCs before and after surface modification. FTIR studies were performed to ensure that surface modification of the NCs was successful. For the black curve, the FTIR spectrum of the oleic acid terminated NCs contains strong -CH_3 bands at 2925 and 2854 cm^{-1}. After ligand exchange to PAA (red line), the decrease of the alkane peaks and the appearance of a strong carbonyl peak at 1716 cm^{-1} suggest that ligand exchange was successful. Upon ligand attachment to PAH (blue line), the decreased carbonyl peak as well as the inconspicuous peak located in 739 cm^{-1} indicate the existence of additional N-H bond.

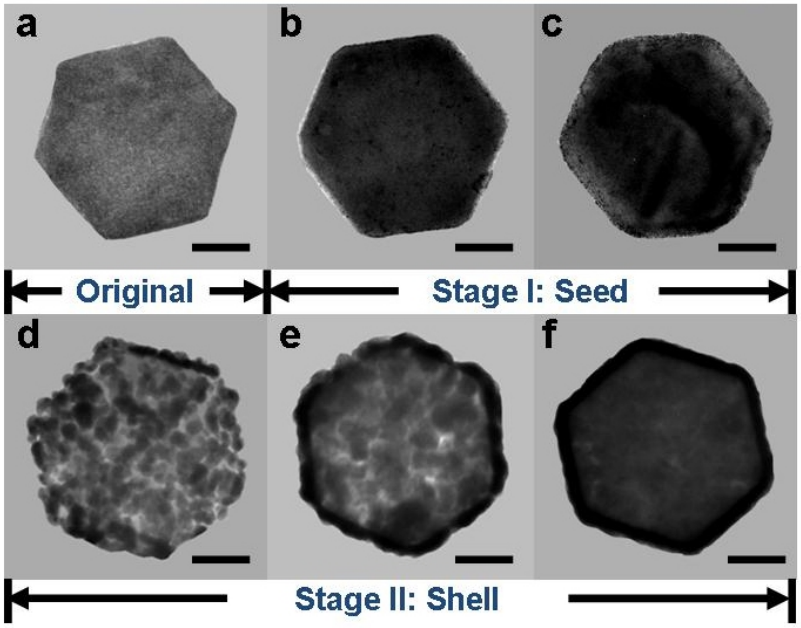

Figure 3-2. Time lapse TEM images of the upconversion NCs during the process of gold seed attachment and shell growth, (a) original, (b-c) with increasing number of attached gold NPs and (d-f) with growing gold nanoshell (Scale Bar: 50 nm).

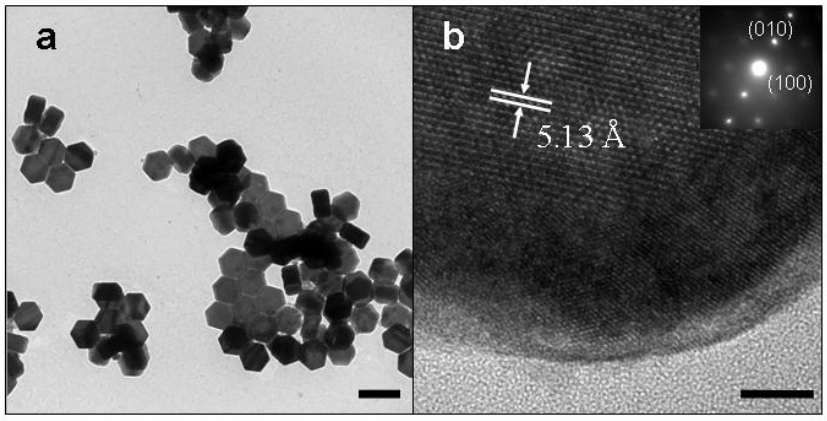

Figure 3-3 (a) TEM, (b and inset) HRTEM and SAED images of $NaYF_4$:Yb/Tm NCs with uniform hexagonal shape (the scale bars correspond to 200 nm in (a) and 5 nm in (b), respectively).

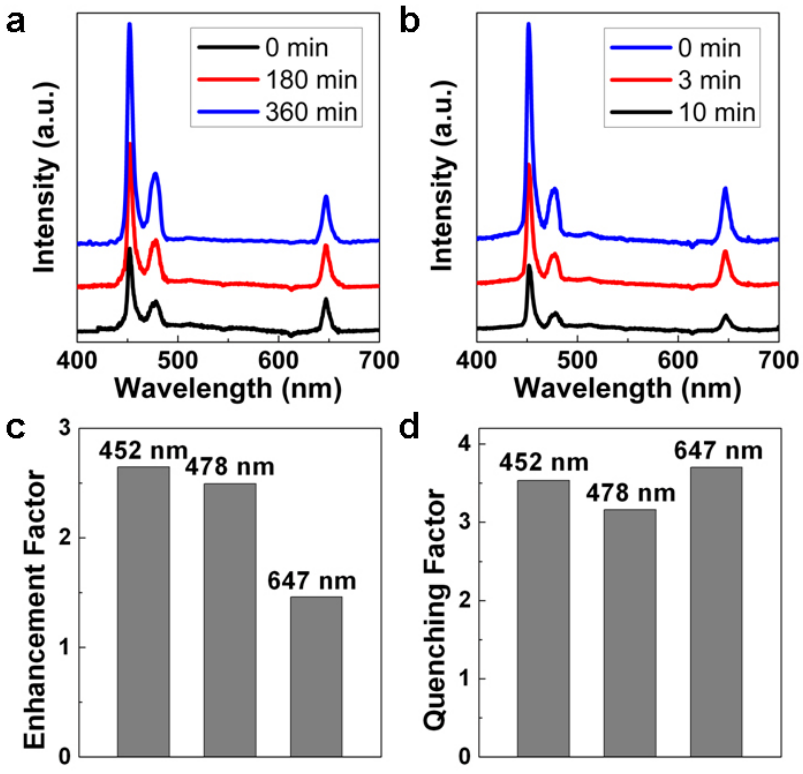

Figure 3-4. Room temperature upconversion emission spectra of $NaYF_4$:Yb/Tm NCs during (a) gold seed attachment stage (0-360 min) and (b) gold shell growth stage (0-10 min). (c) Enhancement factors after gold NPs attachment and (d) quenching factors after gold shell growth at different emission wavelengths.

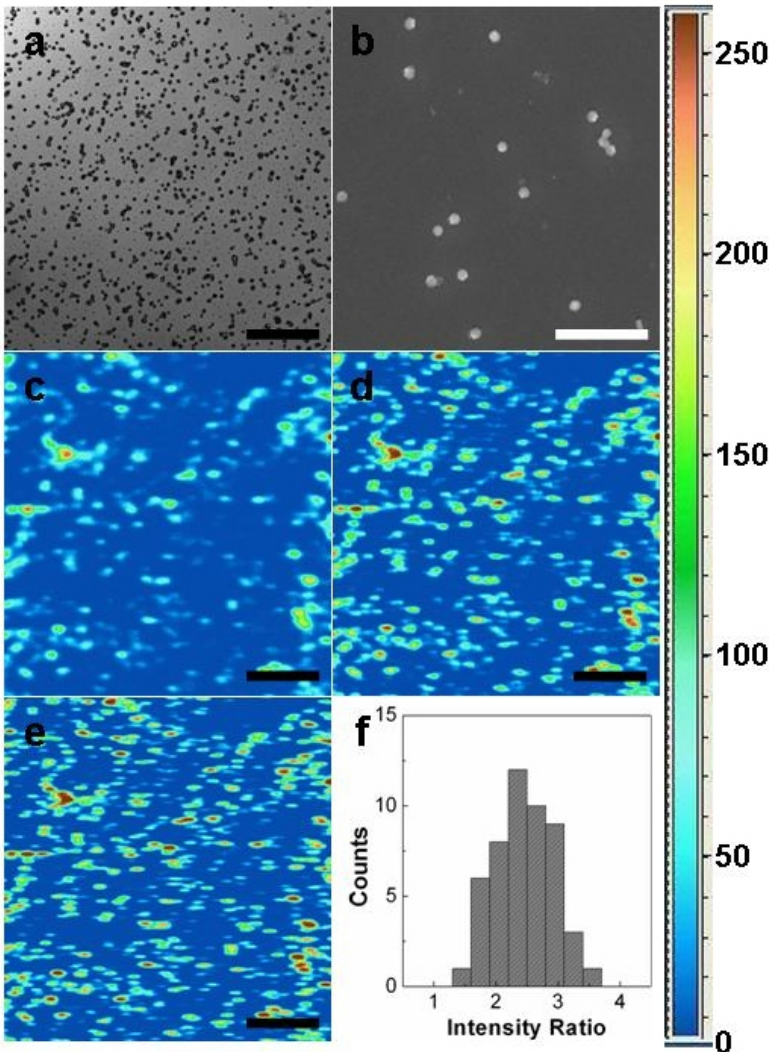

Figure 3-5. (a) Reflection image of NCs on glass substrate. (b) SEM image of a similar sample prepared on silicon wafer. (c-e) Confocal upconversion fluorescence images of the upconversion NCs dipped into gold seed solution for (c) 0 min, (d) 180 min and (e) 360 min. (f) Histogram of the enhancement factors of 50 bright spots (intensity ratio between (e) and (c)). (Scale Bar: 3 μm for b and 20 μm for a,c,d,e)

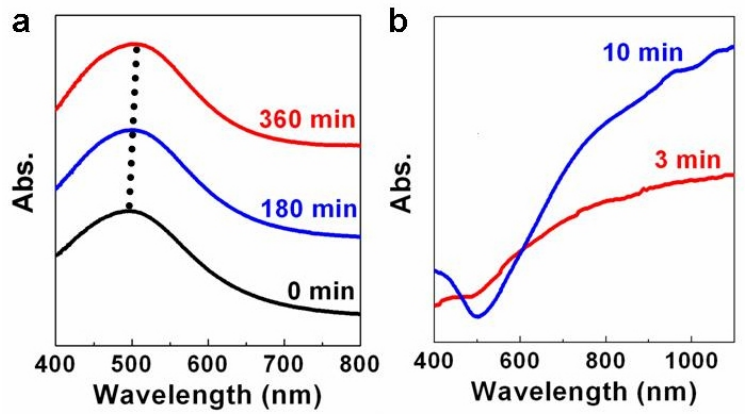

Figure 3-6. UV-Vis spectra of upconversion NCs (a) with gold nanoseeds and (b) with gold shell at different times.

Chapter 4 Spectral Dependent Enhancement of Upconversion Emission with Sputtered Gold Island Films

4.1 Introduction

The ability to tune the spectroscopic properties of fluorophores, especially the enhancement of the emission intensity, by coupling fluorophores with surface plasmonic noble metal nanostructures can lead to exciting opportunities in applications such as sensing technologies and single molecule studies.[1-11] The origin of plasmonic enhancement can be fundamentally attributed to two major effects: (1) an increased excitation rate due to local field enhancement (LFE); (2) an increased emission rate by surface plasmon coupled emission (SPCE), which can change both the fluorescence lifetime and quantum yield.[12-20] In many systems, both factors play important roles in ehancing the emission intensity and are extremely sensitive to the relative spectral position of excitation and emission spectra of the fluorophores versus the plasmonic resonance frequency of the metallic nanostructures. However, it is often difficult to differentiate these two factors, especially in traditional organic dyes with broad overlap in the excitation and emission spectra.[20] In upconversion nanocrystals (NCs) that are able to convert lower energy photons (typically near-infrared (NIR)) into higher energy photons (usually visible), the excitation and emission wavelengths can be substantially different and usually do not have significant overlap.[21,22] Therefore, it allows for the investigation of the interplay between the

excitation-plasmonic resonance or emission-plasmonic resonance coupling, and the possibility to distinguish their effects on the plasmonic enhancement.

Here we report the plasmonic enhancement of the upconversion emission in $NaYF_4$:Yb/Er NCs using gold island films (GIFs). In contrast to isolated gold nanoparticles,[23-26] continuous gold films feature plasmonic resonance wavelengths in the NIR region[27-29] where the excitation wavelength (980 nm) for upconversion NCs is located. Confocal fluorescence images show a more than five-fold overall increase in upconversion emission when coupled with GIFs. Spectroscopic studies indicate that the enhancement is highly spectral dependent with the largest enhancement factor over 12 at selected spectral positions. Excitation power dependence studies suggest the spectral dependent enhancement is closely related to the difference in the excitation process for different emission peaks, in particular the number of excitation photons involved. It is found that high enhancement factors are observed for emission peaks with an excitation process that involves more photons, which is consistent with the increase of effective excitation flux due to LFE. This result indicates that the emission intensity can be significantly modified with noble metal nanostructures and may open exciting opportunities in biomedical imaging, sensing and therapeutics.[30-33]

4.2 Experiment

4.2.1 Synthesis

$NaYF_4$:20%Yb,2%Er NCs was synthesized by thermal decomposition of rare-earth/sodium trifluoroacetate precursors in oleic acid (OA) and octadecene (ODE) as reported previously.[34-41] All chemicals were purchased from Sigma-Aldrich and used without further purification. In a typical procedure, 0.975 mmol of yttrium(III) oxide (Y_2O_3, 99.99%), 0.25 mmol of ytterbium(III) oxide (Yb_2O_3, 99.9%) and 0.025 mmol of erbium(III) oxide (Er_2O_3, 99.9%) were dissolved in 5 ml trifluoroacetic acid (TFA, 99%) in a 100 ml three-necked flask. The slurry was then heated to 80 ^oC with vigorous magnetic stirring under vacuum for 30 minutes to remove water and excessive TFA. Next, 2.5 mmol sodium trifluoroacetate ($NaCOOCF_3$, 98%) was added, along with 7.5 mL of oleic acid (OA, 90%) and 7.5 ml of 1-octadecene (ODE, 90%) at 100 ^oC. Afterwards, the solution was heated to 330 ^oC at a rate of 30 ^oC min^{-1} and maintained at 330 ^oC for 60 minutes to obtain the NCs. The NCs were thoroughly washed and can be readily dispersed in non-polar organic solvents such as chloroform and toluene.

4.2.2 Characterization

The microstructure and composition of the $NaYF_4$:Yb/Er NCs were characterized by a JEOL 6700 FEG scanning electron microscope (SEM), transmission electron microscope (TEM) and energy dispersive X-ray (EDX). The gold island films were prepared by an Anatech LTD Hummer® 6.2 sputtering system. Confocal fluorescence images were taken on a Leica TCS-SP2 AOBS inverted Confocal and Multiphoton

Microscope (Mannheim, Germany) equipped with a Spectra-Physics MaiTai picosecond pulsed infrared laser (Mountain View, CA) set at 980 nm for infrared excitation. Room temperature emission spectra were collected on a Spec-10® system from Princeton Instruments including a liquid-nitrogen cooled CCD camera with variable excitation power density using a 980 nm diode laser. The UV-vis spectra were taken with a Beckman-Coulter spectrophotometer (DU® 800).

4.3 Results and disccsion

4.3.1 Spectrual study

Typically, the as synthesize $NaYF_4$:Yb/Er NCs have a hexagonal plate morphology with uniform size distribution (Fig. 4-1a). As determined by EDX (Fig. 4-1b), the composition of the upconversion NCs is $NaY_{0.723}Yb_{0.25}Er_{0.027}F_4$, slightly different from the nominal targeted composition. The upconversion emission intensity was measured both before and after sputtering of GIFs. To make sure we compare the upconversion emission from the exact same location, photolithography was used to create alignment markers on the glass slide. The upconversion NCs were first spin-coated onto the substrate. The optical image of the NCs on glass slide showed well separated NCs or NC clusters (Fig. 4-2a). Figure 4-2b shows the confocal fluorescence image of the same area in Figure 4-2a, in which each bright spot corresponds to the emission from single NC or a-few-NC clusters. GIFs were then sputtered on the surface of the upconversion

NCs. The average size of the gold island was around 20 nm based on AFM image and SEM image studies (Fig. 4-3). The confocal image of the same area after sputtering GIFs (Fig. 4-2c) clearly shows that the upconversion emission intensity is significantly stronger than that before sputtering GIFs (Fig. 4-2b). Quantitative analysis of the confocal images shows that an average intensity enhancement factor of c.a. 5.1 is achieved, corresponding to a more than 400% increase in the overall emission intensity (Fig. 1d).

To compare the enhancement factors at different spectral positions and further explore the underlying photophysics responsible for the emission modulation, upconversion emission spectra at variable excitation power were monitored before and after sputtering GIFs. Recognizing the significant variations in emission intensity of individual NCs, we have taken spectra from a high density film of NCs obtained using Langmuir–Blodgett (LB) assembly approach[11] (Fig. 4-4). In this case, spectra were taken from an ensemble average of a large number of NCs with the overall intensity variation <20%. To further reduce the impact of location variation and achieve reliable determination of overall spectral enhancement, we have taken and averaged 10 spectra at different locations, both before and after sputtering GIFs (Fig. 4-5) The averaged spectra show three major emission peaks at 522 nm, 550 nm and 652 nm for the upconversion NCs, which are consistent with previous studies on similar NCs.[37] Importantly, a significant increase of upconversion emission intensity is observed at all spectra positions for the NCs with GIFs compared to those without GIFs (Fig. 4-6a).

The plot of emission intensity at three different spectral positions as a function of excitation power density (Fig. 4-6b) reveals several interesting observations: (1) The upconversion NCs with GIFs need significant lower excitation density (~20-30%) than NCs without GIFs to achieve a comparable emission intensity; (2) For NCs without GIFs, a super linear dependence is observed without apparent saturation, while for the NCs with GIFs, a super linear dependence observed at low excitation power density and tends to saturate at high excitation power density; (3) For NC without GIFs, the emission peak at 522 nm is the weakest among three main emission positions throughout the excitation power density range, while for the NCs with GIFs, the 522 nm emission peak was the weakest at low excitation power, but increases much faster with increasing excitation power density and become the strongest emission peak in the end.

It is also interesting to note that the enhancement factors vary significantly with the excitation power (Fig. 4-6c). In general, the enhancement factors first increase and then decrease with increasing excitation power for all three major emission peaks, which can be attributed to the saturation of emission at high excitation power for NCs with GIFs. The enhancement factors are also highly dependent on the exact spectral positions. Specifically, a maximum increase in emission intensity of more than 12 fold is observed at 522 nm, while only a 5 fold enhancement is achieved at 550 nm and 652 nm.

To further understand the relationship between spectral dependent enhancement factors and excitation power density, we have plotted the upconversion emissions intensities *vs.* the excitation power density in the log-log scale, in which the slope

indicates the number of photons responsible for the upconversion process.[21,22] Although in principle, both a 2-photon process and a 3-photon process can result in any of the three emission peaks (Fig. 4-7), the slope of the log-log plot is 2.1 for the 522 nm emission peak, which is larger than those (1.6 and 1.7) of the other two emission peaks (Fig. 4-8a), indicating the 522 emission is more likely to involve 3 photons in the upconversion process. After introducing GIFs onto the upconversion NCs, all the slopes are increased with slope of the 522 nm peak remaining the largest (slope of 2.7, 2.0 and 2.2 for 522, 550 and 653 nm emission peaks). This suggests that the existence of GIFs can also modify the excitation process, which may enhance the upconversion processes involving more photons. Based on these studies, we suggest that LFE is playing an important role here because an increased excitation flux by LFE will impact a more-photon involved upconversion process more significantly. Therefore, the emission intensity at 522 nm can be increased significantly more than the other two emission wavelengths. Meanwhile, the SPEC effect is less likely to be responsible for the large difference in the enhancement factor at different spectral positions because no substantial intensity difference was observed in GIF plasmon resonant spectra among these three different spectral positions (Fig. 4-9).

4.4 Summary

In conclusion, we have observed a plasmonic enhanced upconversion emission with an

average enhancement factor of 5.1 and a largest enhancement factor more than 10 at selected spectral positions. Spectroscopic and excitation power density studies showed that a more-photon-involved upconversion process resulted in a larger enhancement factor, suggesting that the increased excitation flux originated from LFE may be largely responsible for the enhancement disunity at different spectral positions. We believe these studies in upconversion NCs will offer further insight into the plasmonic-exciation-emission interaction between noble metal nanostructures and nanoscale fluorophores, as well as provide a new route to rationally modulate the emission of the fluorophores.

References

1. S. Nie and S. R. Emory, *Science*., 1997, **275**, 1102-1106

2. M. A. Mahmoud and M. A. El-Sayed, *Nano Lett.*, 2009, **9**, 3025-3031

3. A. Campion and P. Kambhampati, *Chem. Soc. Rev*., 1998, **27**, 241-250

4. W. L. Barnes, A. Dereux and T. W. Ebbesen, *Nature*., 2003, **424**, 824-830

5. J. N. Anker, W. P. Hall, O. Lyandres, N. C. Shah, J. Zhao and R. P. Van Duyne, *Nature Materials*, 2008, **7**, 442-453

6. M. C. Daniel and D. Astruc, *Chem. Rev.*, 2004, **104**, 293-346

7. F. Le, D. W. Brandl, Y. A. Urzhumov, H. Wang, J. Kundu, N. J. Halas, J. Aizpurua and P. Nordlander, *ACS Nano.,* 2008, **2**, 707-718

8. K. G. Thomas and P. V. Kamat, Acc. *Chem. Res*., 2003, **36**, 888-898

9. Y. Zhang, F. Huang, Y. Chi and A. K. Y. Jen, *Adv. Mater.*, 2008, **20**, 1565

10. B. Kokuoz, J. R. DiMaio, C. J. Kucera, D. D. Evanoff, Jr. and J. Ballato, *J. Am. Chem. Soc.*, 2008, **130**, 12222

11. A. Tao, P. Sinsermsuksakul and P. Yang, *Nat. Nanotech*., 2007, **2**, 435-440.

12. W. Feng, L. D. Sun and C. H. Yan, *Chem. Commun.*, 2009, **29**, 4393-4395

13. P. Anger, P. Bharadwaj and L. Novotny, *Phys. Rev. Lett.*, 2006, **96**

14. R. Bardhan, N. K. Grady, J. R. Cole, A. Joshi and N. J. Halas, *ACS Nano*, 2009, **3**, 744-752

15. J. Q. Gu, J. Shen, L. D. Sun and C. H. Yan, *J. Phys. Chem. C*, 2008, **112**, 6589-6593

16. K. Ray, R. Badugu and J. R. Lakowicz, *J. Am. Chem. Soc.*, 2006, **128**, 8998-8999

17. S. Schietinger, T. Aichele, H. Q. Wang, T. Nann and O. Benson, *Nano Lett.*, 2010, **10**, 134-138

18. A. Kinkhabwala, Z. F. Yu, S. H. Fan, Y. Avlasevich, K. Mullen and W. E. Moerner, *Nat. Photo.,* 2009, **3**, 654-657

19. P. P. Pompa, L. Martiradonna, A. Della Torre, F. Della Sala, L. Manna, M. De Vittorio, F. Calabi, R. Cingolani and R. Rinaldi, *Nat. Nanotech.*, 2006, **1**, 126-130.

20. Y. Chen, K. Munechika and D. S. Ginger, *Nano Lett.*, 2007, **7**, 690-696

21. F. Auzel, *Chem. Rev.*, 2004, **104**, 139-173

22. D. R. Gamelin and H. U. Gudel, in *Transition Metal and Rare Earth Compounds: Excited States, Transitions, Interactions Ii*, 2001, pp. 1-56

23. W. A. Murray and W. L. Barnes, *Adv. Mater.*, 2007, **19**, 3771-3782

24. Y.N. Xia and N. J. Halas, *Mrs Bull.,* 2005, **30**, 338-344

25. J. F. Li, Y. F. Huang, Y. Ding, Z. L. Yang, S. B. Li, X. S. Zhou, F. R. Fan, W. Zhang, Z. Y. Zhou, D. Y. Wu, B. Ren, Z. L. Wang and Z. Q. Tian, *Nature*, 2010, **464**, 392-395

26. W. H. Ni, T. Ambjornsson, S. P. Apell, H. J. Chen and J. F. Wang, *Nano Lett.*, 2010, **10**, 77-84

27. H. Wang, G. P. Goodrich, F. Tam, C. Oubre, P. Nordlander and N. J. Halas, *J. Phys. Chem. B,* 2005, **109**, 11083-11087

28. J. W. Bai, S. X. Huang, L. Y. Wang, Y. Chen and Y. Huang, *J. Mater. Chem.*, 2009, **19**, 921-923

29. L. Y. Wang, J. W. Bai, Y. J. Li and Y. Huang, *Angew. Chem.-Int. Edit.*, 2008, **47**, 2439-2442

30. L. Y. Wang, R. X. Yan, Z. Y. Hao, L. Wang, J. H. Zeng, H. Bao, X. Wang, Q. Peng and Y. D. Li, *Angew. Chem.-Int. Edit.*, 2005, **44**, 6054-6057

31. F. van de Rijke, H. Zijlmans, S. Li, T. Vail, A. K. Raap, R. S. Niedbala and H. J. Tanke, *Nat. Biotechnol.*, 2001, **19**, 273-276

32. J. Hampl, M. Hall, N. A. Mufti, Y. M. Yao, D. B. MacQueen, W. H. Wright and D. E. Cooper, *Anal. Biochem.*, 2001, **288**, 176-187

33. S. F. Lim, R. Riehn, W. S. Ryu and N. Austin, *Nano. Lett.*, 2006, **6**, 169-174

34. J. C. Boyer, L. A. Cuccia and J. A. Capobianco, *Nano Lett.*, 2007, **7**, 847-852

35. H. X. Mai, Y. W. Zhang, L. D. Sun and C. H. Yan, *J. Phys. Chem. C,* 2007, **111**, 13721-13729

36. F. Wang and X. G. Liu, *J. Am. Chem. Soc.*, 2008, **130**, 5642-5643

37. H. Zhang, Y. J. Li, I. A. Ivanov, Y. Q. Qu, Y. Huang and X. F. Duan, *Angew. Chem.-Int. Edit.*, 2010, **49**, 2865-2868

38. Z. Q. Li, Y. Zhang and S. Jiang, *Adv. Mater.*, 2009, **21**, 4768-4768

39. W. B. Niu, S. L. Wu, S. F. Zhang and L. Li, *Chem. Commun.*, 2010, **46**, 3908-3910

40. S. Heer, K. Kompe, H. U. Gudel and M. Haase, *Adv. Mater.*, 2004, **16**, 2102-2105

41. G. S. Yi and G. M. Chow, *Adv. Funct. Mater.,* 2006, **16**, 2324-2329

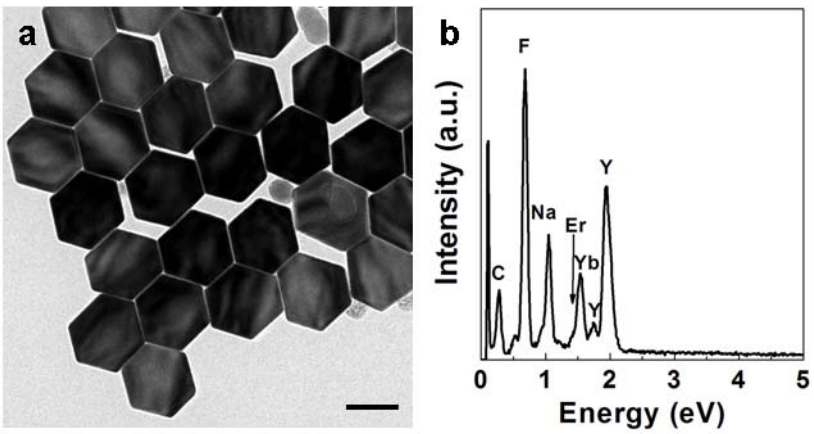

Figure 4-1. (a) TEM image of upconversion NCs. (Scale Bar: 200 nm) (b) EDX spectrum of upconversion NCs shows only sodium, fluorine and rare-earth elements. The carbon signal comes from the carbon membrane on TEM grid. The atomic ratio of Y:Yb:Er is 72.3:25.0:2.7

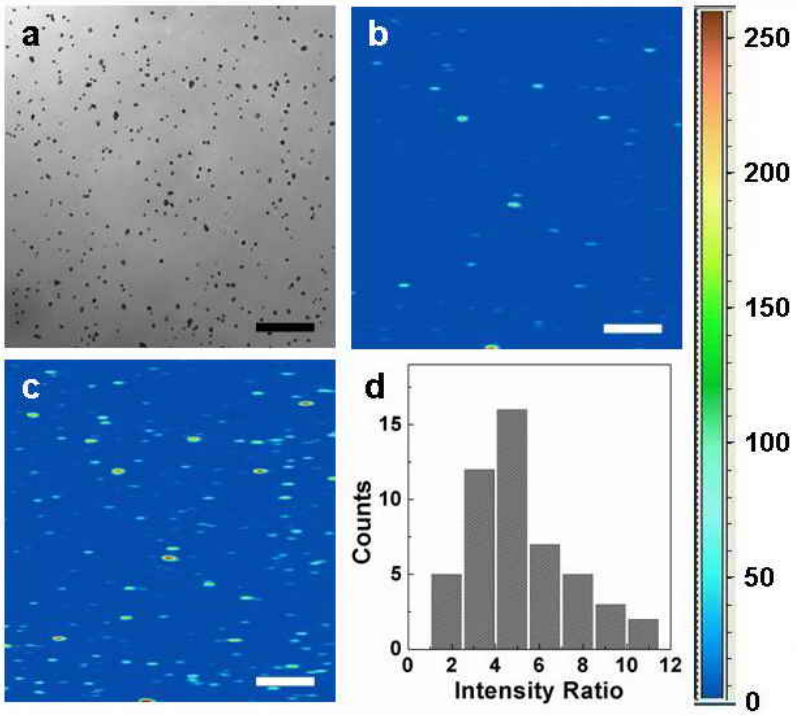

Figure 4-2. (a) Reflection image of upconversion NCs on glass slide. (b, c) Confocal upconversion fluorescence images of the upconversion NCs on glass slide before (b) and after (c) gold sputtering obtained with 980 nm excitation. (d) Histogram of the enhancement factors of 50 bright spots (intensity ratio between (b) and (c)). (Scale Bar: 2 μm for a, b, c and 100 nm for inset)

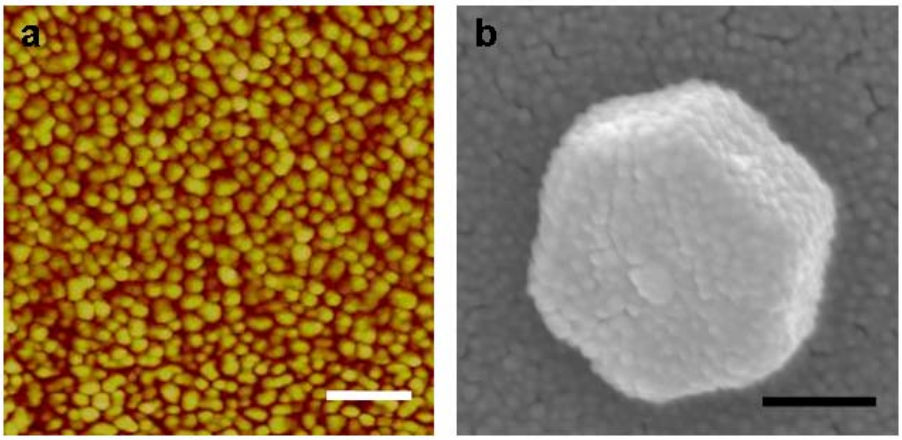

Figure 4-3. (a) AFM image of a glass slide sputtered with gold island film; (b) SEM image of a single upconversion NCwith sputtered gold island filems. (Scale Bar: 100 nm)

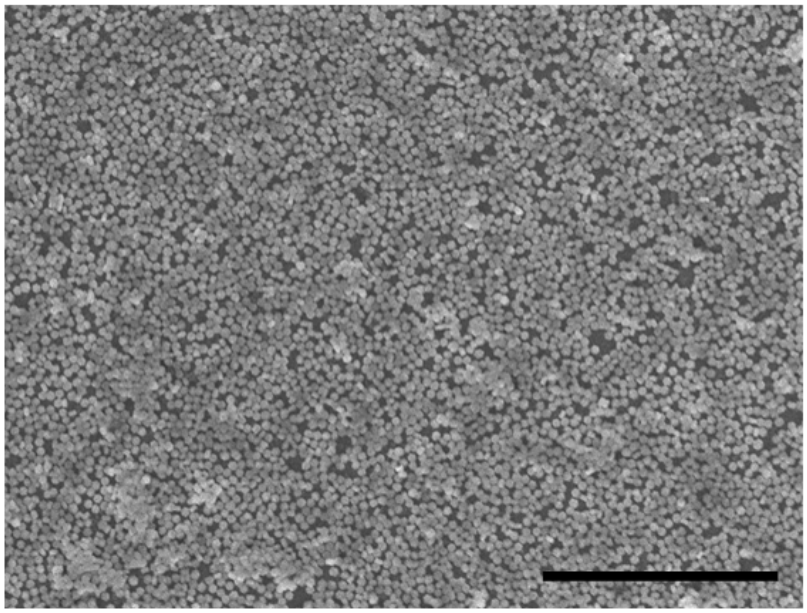

Figure 4-4. SEM image of a large area of upconversion NCs prepared by Langmuir–Blodgett (LB) assembly. (Scale Bar: 10 μm)

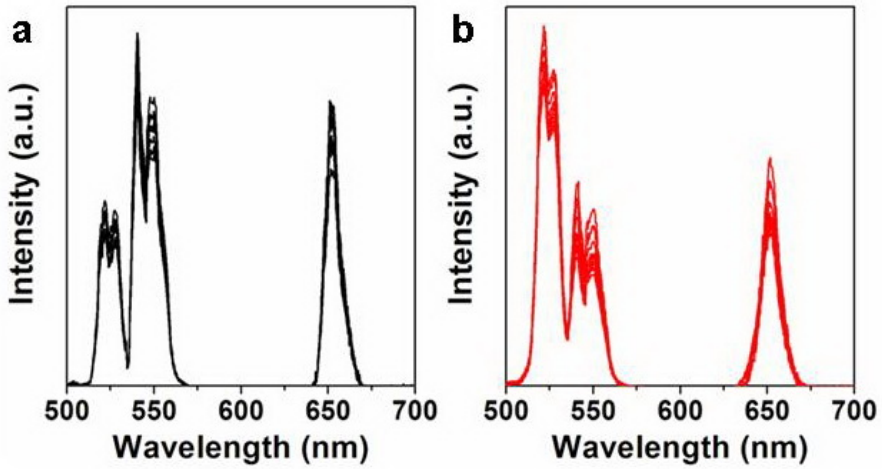

Figure 4-5. Emission spectra obtained from 10 different locations in L-B assembled upconversion NC film before (a) and after (b) GIFs sputtering.

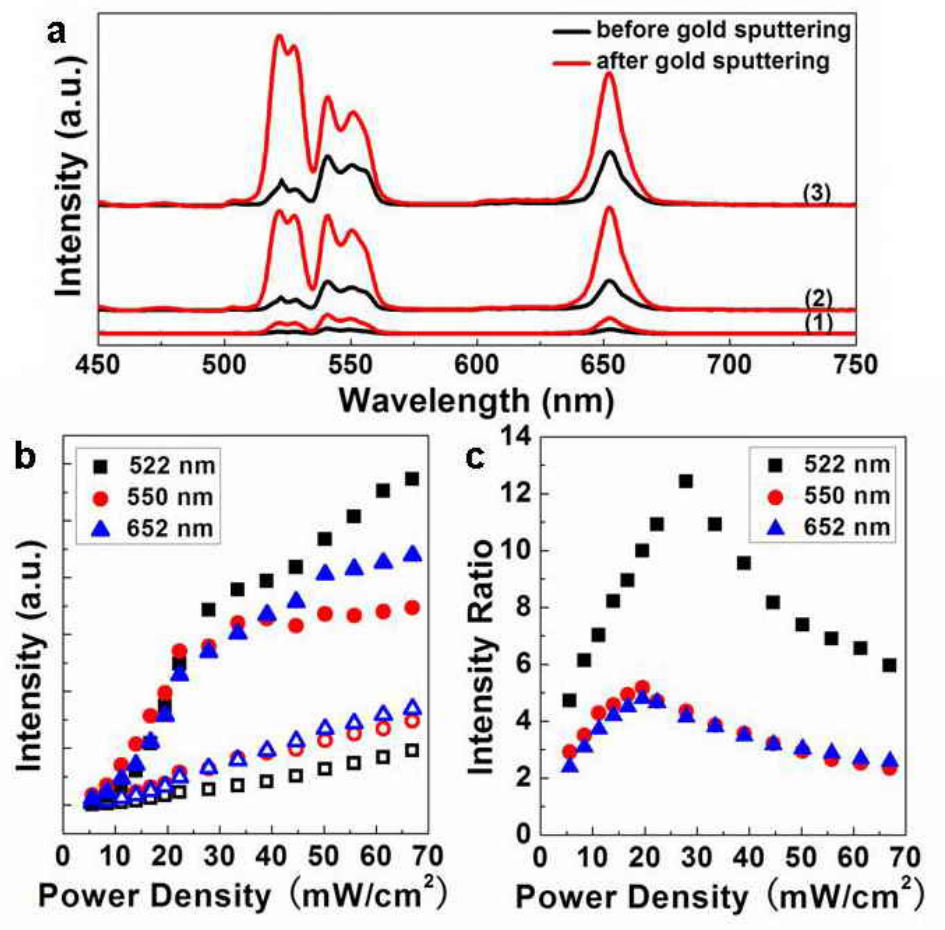

Figure 4-6. (a) Emission spectra of upconversion NCs on glass slide before and after gold sputtering excited with a 980 nm diode laser at the power density of 11 mW/cm2, 40 mW/cm2 and 67 mW/cm2 for (1), (2) and (3) respectively. (b) Power dependent upconversion emission before (open) and after (solid) gold sputtering. (c) Power dependent enhancement factor of upconversion emission on glass slide at different wavelengths.

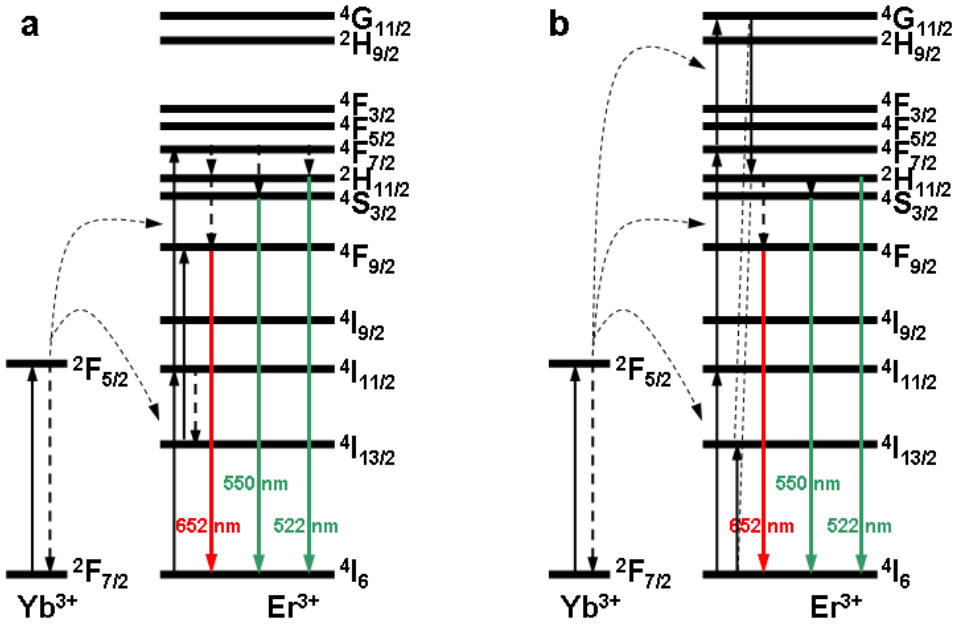

Figure 4-7. Schematic illustration of the two-photon (a) and three-photon (b) upconversion process in $NaYF_4$:Yb,Er NCs.

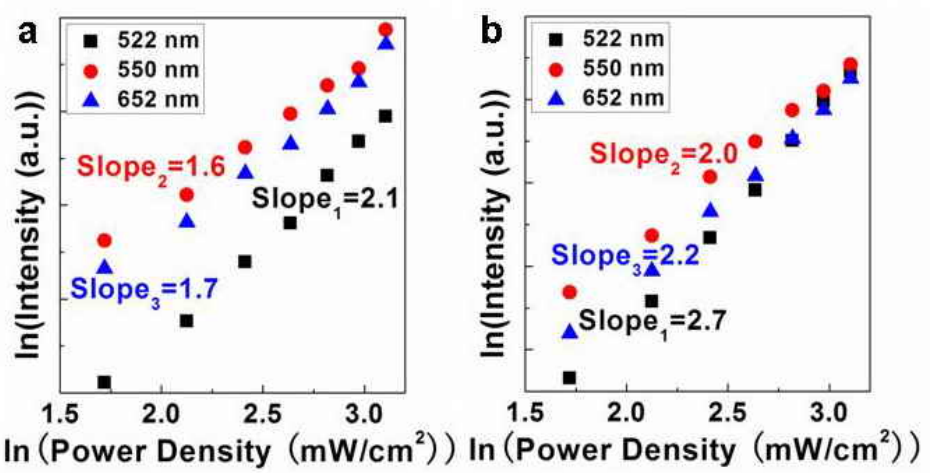

Figure 4-8. Power dependence of upconversion emission on glass slide excited with a 980 nm diode laser before (a) and after (b) gold sputtering. Only data before saturation is presented here.

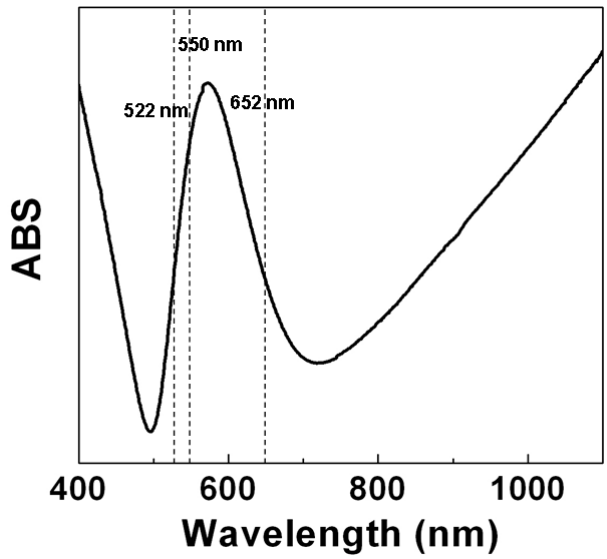

Figure 4-9. UV-Vis spectrum of the gold island film sputtered on a glass slide.

Chapter 5 Further Study and Conclusion

Upconversion nanocrystals have been used in various application from bio-imaging to energy harvesting. However, the wider application of UCNCs has been limited by their ratherly low quantum yield (usually 0.02 % - 2 %). Substantial efforts have been made to fine tune the spectral properties of UCNCs by controlling the crystal phase, physical morphology and size, dopant types and concentrations.

Alternatively, plasmonic structures (e.g. Au nanoparticles or Au thin films) have also been explored to couple with the UCNCs and proven to be an effective way to enhance the upconversion fluorescence by up to 5 times. However, the enhancement factor was generally small (less than 5 folds), and the fabrication methods were relatively complicated, involving several steps of surface modification or coating.

Here, we propose a systematic study of plasmonic modulation of upconversion emission with silver thin films, to achieve an exceptionally large emission enhancement (>16 fold) and a precise spectral control. The coupling of UCNCs with plasmonic silver thin films can be simply achieved by a spin-coating process. The substantial difference between the excitation and emission wavelengths allows us to independently investigate the impact of plasmonic coupling on the excitation and emission process using detailed spectroscopic study. The detailed mechanism for plasmonic coupling is further investigated using electrostatic simulation by solving Maxwell equations.

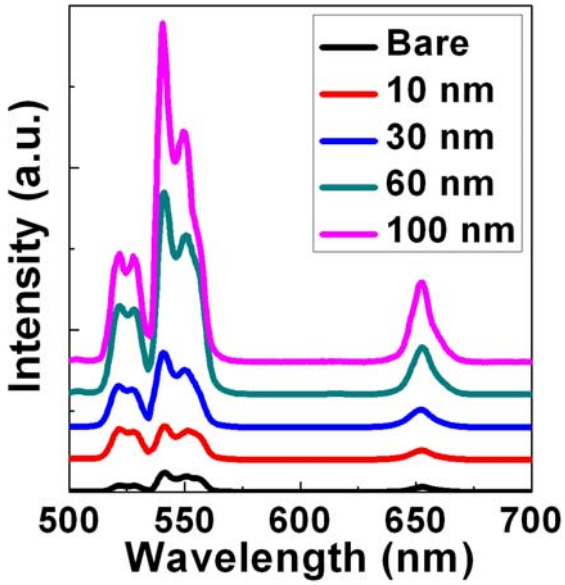

Figure 1| Emission spectra of upconversion nanocrystals (UCNCs) on silver thin films with different thichnesses.